

Scrambling Dynamics and Out-of-Time Ordered Correlators in Quantum Many-Body Systems: a Tutorial

Shenglong Xu¹ and Brian Swingle^{2,3}

¹*Department of Physics & Astronomy, Texas A&M University, College Station, Texas 77843, USA*

²*Department of Physics, Brandeis University, Waltham, Massachusetts 02453, USA*

³*Department of Physics, University of Maryland, College Park, Maryland 20742, USA*

This tutorial article introduces the physics of quantum information scrambling in quantum many-body systems. The goals are to understand how to quantify the spreading of quantum information precisely and how causality emerges in complex quantum systems. We introduce the general framework to study the dynamics of quantum information, including detection and decoding. We show that the dynamics of quantum information is closely related to operator dynamics in the Heisenberg picture, and, in certain circumstances, can be precisely quantified by the so-called out-of-time ordered correlator (OTOC). The general behavior of OTOC is discussed based on several toy models, including the Sachdev-Ye-Kitaev model, random circuit models, and Brownian models, in which OTOC is analytically tractable. We introduce numerical methods, both exact diagonalization and tensor network methods, to calculate OTOC for generic quantum many-body systems. We also survey current experiment schemes to measure OTOC in various quantum simulators.

CONTENTS

I. Introduction	1	B. Tensor-network methods	26
II. Basic setup of scrambling dynamics	2	VIII. Experimental Schemes	29
A. Alice-Bob communication protocol: the significance of commutators	3	A. Rewinding time	29
B. Bound on commutators	3	B. Randomized measurement	30
C. Two central goals: detection and recovery	5	IX. Epilogue	31
III. Quantum information formulation	6	X. Acknowledgement	33
A. Entanglement spreading	6	References	33
B. Alice-Bob communication again	8	Appendix A. Useful definitions, operator identities and entropy inequalities	36
C. Quantum mutual information from random unitary dynamics	9	1. Matrix norm	36
IV. Hayden-Preskill protocol: detecting and recovering the information	10	2. Entropy inequalities	37
A. Detecting the information front	11	3. Operator identities	37
B. Recovering the information: many-body teleportation	13	Appendix B. Operator strings and OTOC in qudit systems and majorana systems	37
V. Microscopic physics of operator growth	15	1. OTOC in qudit system	37
A. Relating OTOC to operator dynamics	15	2. OTOC in majorana systems	37
B. Scrambling dynamics in geometrically local systems	17	Appendix C. Lieb-Robinson bound	38
VI. Scrambling dynamics in systems with short-ranged interaction	18		
A. Prototype models	19		
1. Free fermions	20		
2. coupled Sachdev-Ye-Kitaev model	20		
3. Random circuit model	21		
4. Brownian models	22		
B. Phenomenological description	23		
VII. Numerical methods	25		
A. Exact diagonalization and Krylov space method	25		

I. INTRODUCTION

Recent years have seen remarkable developments in laboratory platforms for studying quantum physics. Systems ranging from ultracold atoms, trapped ions, superconducting qubits to universal quantum computers now provide exciting opportunities to study quantum many-body physics that was out-of-reach before. One frontier concerns long-time coherent quantum many-body dynamics in closed systems, which has drawn extensive research interests from multiple communities, such as condensed matter, AMO, quantum information science and

high energy physics. Synergistic experimental and theoretical research has revealed a series of discoveries in the arena of quantum dynamics. Moreover, these platforms expand the scope of the traditional condensed matter physics, and demand new tools and frameworks to study quantum many-body systems that are far from equilibrium (see [1] for a recent overview on quantum simulators and references therein).

In the simplest kind of “quench” experiment one prepares an initial state, designs a Hamiltonian or unitary circuit to evolve the state, and measures the final state. While the freedom in the initial state and engineered dynamics largely depends on the specific experimental platform, this general class of experiments certainly raises questions regarding the general behavior of quantum many-body dynamics when the initial state is far away from equilibrium. Consider a simple product initial states of qubits, with each qubit in $|0\rangle$ or $|1\rangle$. Now let the state evolve under a generic unitary operator. The general expectation is that the state will not remain a product state but will instead become a complicated superposition of product states.

One way to track the complexity is to monitor the buildup of entanglement in the state. Entanglement can be quantified using the tool of entanglement entropy. Given a subregion A of the system, one can obtain the density matrix by tracing out the complement \bar{A} ,

$$\rho_A = \text{tr}_{\bar{A}} |\psi\rangle \langle \psi|. \quad (1)$$

The entanglement entropy of A is defined as

$$S(A) = -\text{tr} \rho_A \log_2 \rho_A. \quad (2)$$

It is also straightforward to show that $S(A) = S(\bar{A})$ when the total state is pure.

In a quench experiment starting from a product state, $S(A)$ will begin at zero and then grown over time. This growth indicates that the density matrix is becoming more mixed, which corresponds to an increasingly feature state of subsystem A . In fact, based on statistical considerations, we expect that the density matrix should approach a maximally mixed state if the evolving unitary is generic. In other words, in the late time, the subsystem thermalizes by entangling with its environment. If instead of a totally generic evolution we consider a system that conserves energy, then the late time density matrix is expected to approach a thermal state with temperature determined by the initial state via its average energy.

Once ρ_A thermalizes, it only depends on macroscopic quantities such as energy or charge, while microscopic information about the initial state is apparently lost [2–6]. Two orthogonal initial states with the same energy or charge density would thermalize to the same local density matrix, and so one would be unable to distinguish them locally. On the other hand, the two states remain orthogonal since the dynamics is unitary and are always distinguishable if global information about the two states is accessible. Thermalization and unitary dynamics suggest that the initial state’s information becomes non-local

under time evolution: it flows into more and more non-local degrees of freedom and cannot be recovered by local probes. This process of information flow from local to non-local degrees of freedom is called quantum information scrambling. It was initially studied in black hole dynamics [7–10] and later extended to general quantum many-body systems [11–13].

In this tutorial, we discuss scrambling dynamics in general quantum many-body systems in detail. We will argue that just like a piece of metal can be characterized by its transport properties associated with the electrons, a generic quantum body-body system can be characterized by its transport properties associated with quantum information. Given existing perspective articles on related topics [14, 15] which give the basic intuition, this tutorial aims to provide a more in-depth discussion. The remainder of the tutorial is organized as follows. In Sec. II, we discuss the basic setup of scrambling dynamics based on an Alice-Bob communication protocol. In Sec. III, we discuss how to quantify scrambling dynamics using entanglement entropy measures and provide the basic intuition using random unitary dynamics. In Sec. IV, we discuss the Hayden-Preskill protocol, which is a special case of the general setup, and show that in this case, the scrambling dynamics can be quantified by the out-of-time ordered correlator (OTOC). In Sec. V, we relate scrambling and OTOC to operator dynamics and survey OTOC in systems with few-body interactions. In Sec. VI, we discuss the behavior of OTOC in systems with short-ranged interactions in detail based on several toy models. In Sec. VII, we discuss numerical tools available to calculate OTOC for general systems. In Sec. VIII, we survey various experimental schemes to measure OTOC.

II. BASIC SETUP OF SCRAMBLING DYNAMICS

We start by specifying our prototype quantum many-body system. For concreteness, let us consider a system of N qubits. Each qubit has a basis spanned by $|0\rangle$ and $|1\rangle$. On each two-level system, one can define a complete basis of operators, which are the identity and the Pauli operators, which in matrix representation are

$$I = \begin{pmatrix} 1 & 0 \\ 0 & 1 \end{pmatrix}, \sigma^x = \begin{pmatrix} 0 & 1 \\ 1 & 0 \end{pmatrix}, \sigma^y = \begin{pmatrix} 0 & -i \\ i & 0 \end{pmatrix}, \sigma^z = \begin{pmatrix} 1 & 0 \\ 0 & -1 \end{pmatrix}. \quad (3)$$

The total Hilbert space is a tensor product of local Hilbert spaces and has dimension 2^N . In some parts of the tutorial, we will generalize the situation of qudits with local Hilbert space dimension q or Majorana fermion systems, but let us stay with qubits for now.

Given an initial state in the system $|\psi\rangle$, its dynamics is described by a unitary time evolution operator

$$|\psi(t)\rangle = U(t) |\psi\rangle, \quad (4)$$

where so far $U(t)$ is an arbitrary family of unitary matrices acting on the total Hilbert space. We will later

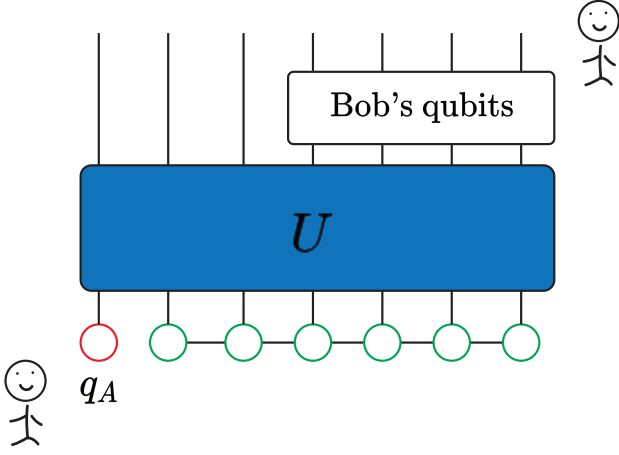


FIG. 1. Alice and Bob try to communicate through a strongly interacting system of N qubits. The time evolution of the system is described by an unitary operator U . Alice has full control of the first qubit q_A and Bob has access to a set of qubits in the system, but not all of them.

assign $U(t)$ more structure. The simplest quench experiment corresponds to choosing an initial $|\psi\rangle$, choosing a dynamics $U(t)$, and choosing a set of observables to measure in the final state $U(t)|\psi\rangle$.

A. Alice-Bob communication protocol: the significance of commutators

Now let us consider the scenario illustrated in Fig. 1. Alice owns one of the N qubits, denoted by q_A , that she has full control over. Bob owns a set of qubits denoted by B . Starting with an initial state $|\psi\rangle$, Alice wants to send a bit $a \in \{0, 1\}$ to Bob. Depending on a , Alice flips her qubit by applying the $\sigma_{q_A}^x$ operator to the state, or does nothing. The system then evolves for a time t . Finally, Bob makes a measurement O_B of his qubits to try to learn whether Alice flipped the spin or not.

The expectation value of Bob's measurement given that Alice does not flip her qubit is

$$\langle O_B \rangle_0 = \langle \psi | U^\dagger O_B U | \psi \rangle = \langle \psi(t) | O_B | \psi(t) \rangle. \quad (5)$$

Alice can also flip her qubit, and then the expectation value of Bob's measurement is

$$\begin{aligned} \langle O_B \rangle_1 &= \langle \psi | \sigma_{q_A}^x U^\dagger O_B U \sigma_{q_A}^x | \psi \rangle \\ &= \langle \psi(t) | \sigma_{q_A}^x(-t) O_B \sigma_{q_A}^x(-t) | \psi(t) \rangle. \end{aligned} \quad (6)$$

where $\sigma^x(-t) = U \sigma^x U^\dagger$ is a Heisenberg operator. Let us assume that whatever Alice does, she repeats it many times, so that Bob can obtain the expectation value of his measurements. The difference between $\langle O_B \rangle_0$ and $\langle O_B \rangle_1$ is

$$\langle O_B \rangle_0 - \langle O_B \rangle_1 = \langle \psi(t) | \sigma^x(-t) [\sigma^x(-t), O_B] | \psi(t) \rangle, \quad (7)$$

where we used the operator identity $\sigma^x(-t)\sigma^x(-t) = I$.

Let us pause to understand the physics. Whenever the difference is small, then Bob cannot tell whether Alice flipped the qubit or not. In this case, very little information is transmitted from Alice to Bob since what Bob measures is nearly independent of what Alice did. So we want to understand the size of the difference.

Using the Cauchy-Schwarz inequality (We provide a list of useful inequalities in the appendix A 2), we can bound the difference by

$$\begin{aligned} |\langle O_B \rangle_1 - \langle O_B \rangle_0|^2 &\leq \langle \psi(t) | [\sigma_{q_A}^x(-t), O_B]^\dagger [\sigma_{q_A}^x(-t), O_B] | \psi(t) \rangle \\ &\leq \|[\sigma_{q_A}^x(-t), O_B]\|_\infty^2 \end{aligned} \quad (8)$$

where $\|O\|_\infty$ is the operator norm defined as the square root of largest eigenvalue of the positive Hermitian operator $O^\dagger O$. The first inequality is from Cauchy-Schwarz and the second inequality is from the definition of the operator norm. Definitions of various matrix norms of operators are given in Sec. A 1. Therefore, the difference of Bob's measurement between Alice flipping her qubit or not is bounded by the operator norm of the commutator $[\sigma^x(-t), O_B]$. This statement is independent of the initial state $|\psi\rangle$ Alice and Bob choose as the medium to attempt to transmit the information.

The bound has a very intuitive picture. At $t = 0$, σ^x only has support on Alice's qubit and does not overlap with Bob's qubits. Therefore, the commutator is zero initially, and no matter what Bob does to his qubits, he cannot tell whether Alice flips her qubit. He can do no better than random guessing when trying to determine Alice's bit. As t increases, $\sigma^x(-t)$ starts to grow as a Heisenberg operator, acting on more qubits. Whenever the supports of $\sigma^x(-t)$ and O_B start to overlap, their commutator becomes nonzero, and Bob has a chance to tell whether Alice flipped her qubit.

B. Bound on commutators

A natural first question is whether fundamental bounds exist on the norm the commutators given t and r , which is the separation between q_A and B . There are many possible behaviors for the commutator of local operators in a quantum many-body system. For example, one might expect very different behavior between integrable and chaotic models, between non-interacting and strongly interacting models, and between localized and delocalized models.

One is probably familiar with at least one such constraint, namely the limitation on communication imposed by the speed of light. In the modern language of quantum field theory, this is called microcausality. It states that, given any two physical local operators $W(x)$ and $V(y)$ located at spacetime points x and y , their commutator

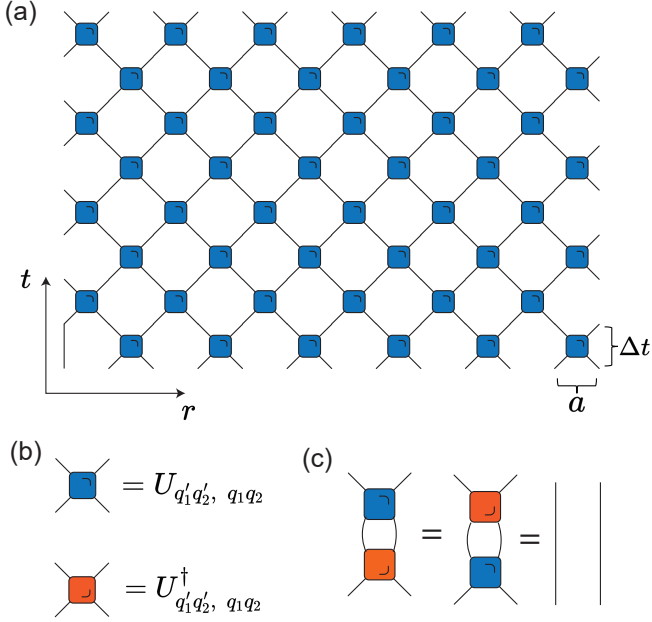


FIG. 2. The tensor network representation of unitary circuit with spatial locality built in.

must vanish if x and y are ‘spacelike separated’,

$$x, y \text{ spacelike separated} \rightarrow [W(x), V(y)] = 0, \quad (9)$$

In other words, if y is outside of the ‘light cone’ of space-time point x , then the corresponding operators must exactly commute. Crucially, this is an operator statement and hence a state-independent bound on information propagation. It is a fundamental property of any unitary Lorentz invariant local quantum field theory.

There is somewhat analogous property for many lattice models which do not have relativistic causality built in microscopically. As discussed earlier, the commutator is zero when O_B is outside the support of the Heisenberg operator $\sigma^x(-t)$. Therefore the support $\sigma^x(-t)$ which grows as a function of time serves as an emergent “light-cone” for the lattice models, which describes how fast information can propagate in these systems. To provide an explicit example of the emergent lightcone, let us consider the unitary time evolution operator with a tensor network structure built from local two-qubit unitary gates, as sketched in Fig. 2. This unitary operator describes the time evolution of a spin chain with nearest neighboring interaction, without relativistic causality built in but only locality. Given the brickwork structure of U , the tensor network representation of a Heisenberg

operator, say $\sigma^x(-t) = U\sigma^x U^\dagger$, is

$$\sigma^x(-t) = \text{[Tensor network diagram]} \quad (10)$$

Each blue or orange block represents a local unitary matrix, and the green block represents the σ^x at $t = 0$. The blue block and orange block are unitaries conjugate to each other. As a result, if a blue block and an orange block are directly connected, they are replaced by straight lines, representing identity operators. The tensor network after this transformation is

$$\sigma^x(-t) = \text{[Tensor network diagram]} \quad (11)$$

The remaining blocks (non-shaded region) form a linear lightcone, visualizing the growth of the Heisenberg operator over time. The effective speed of light is $a/\Delta t$, where a is the lattice constant and Δt is the time scale associated with one layer of the unitary circuit. This is a simple but remarkable result, showing that an effective linear lightcone can emerge from the locality in systems without microscopic relativistic causality. The commutator $[\sigma^x(-t), O_B]$ is strictly zero when O_B is outside the emergent lightcone.

There is one caveat to generalize this approach to obtain the speed limit for a static Hamiltonian. For instance, consider a Hamiltonian describing nearest neighboring interactions between qubits.

$$H = \sum_r H_{r,r+1} \quad (12)$$

One can trotterize the time evolution operator $\exp(-iHt)$ to the local tensor structure shown in Fig. 2. Each local unitary block takes the form $u = \exp(-iH_{r,r+1}\Delta t)$. The tensor structure in Fig. 2 approaches to $\exp(-iHt)$ in the limit $\Delta t \rightarrow 0$. Then the velocity $a/\Delta t$ from the tensor structure goes to infinity, which is not a meaningful bound. Nevertheless, for discrete models with a local Hamiltonian and a finite local Hilbert space dimension, one can establish a much tighter linear lightcone with finite speed of the commutator using a more sophisticated approach originally due to Lieb and Robinson, which we discuss in appendix C. This bound, now usually referred to as the Lieb-Robinson bound [16],

states that for two local operators $W(r)$ and $V(r')$ at (spatial) position r and r' respectively, we have the following bound on the operator norm of the commutator,

$$\frac{\| [W(r, t), V(r', 0)] \|_\infty}{\|W\|_\infty \cdot \|V\|_\infty} \leq a e^{\lambda \left(t - \frac{|r-r'|}{v_{LR}} \right)}. \quad (13)$$

where a , λ and v_{LR} depend on the microscopic parameters of the Hamiltonian. This inequality, combined with Eq. (8), bounds the difference of the signal that Bob measures at time t to determine whether Alice flips her qubit at time $t = 0$. Observe that if the distance $|r' - r| \geq v_{LR}t$, the bound, although not zero, is exponentially small, indicating that it is almost impossible for Bob to tell whether what Alice did. This establishes an approximate lightcone with a finite speed v_{LR} , called the Lieb-Robinson velocity, for local systems without relativistic causality.

C. Two central goals: detection and recovery

The Lieb-Robinson bound is independent of the state $|\psi\rangle$ and is universally applicable. Its importance lies in proving that information cannot travel super ballistically in quantum many-body systems with short-ranged interaction. However, in many cases, the bound can be quite loose, just like the physical speed of light is a loose bound on how fast an object moves in our universe. Moreover, it does not provide a way to calculate v_{LR} but only proves that it is finite. Therefore we need an operational approach to calculate how fast information spreads for a given system—the information lightcone (we will provide a precise definition of the information lightcone in the next section). For now, we can interpret the information lightcone as the minimal set of qubits, outside of which none of Bob's measurements can distinguish Alice's actions at $t = 0$. This set only contains Alice's qubit q_A at $t = 0$ but the set grows over time. One of the central goals in studies of scrambling dynamics is to calculate the linear size of this region as a function of t . The Lieb-Robinson bound provides an upper bound $R(t) \leq v_{LR}t$ for local Hamiltonians.

A key second goal is to determine Bob's optimal measurement to capture the signal sent by Alice, or to find the optimal O_B to maximize the difference between $\langle O_B \rangle_0$ and $\langle O_B \rangle_1$. In non-interacting or weakly interacting systems, the excitation created by Alice can remain coherent for a long time and propagates with a group velocity determined by the underlying medium. Imagine a wave packet of an electron or a magnon moving through a metal or a magnet. In this case, Bob can easily tell whether Alice made the excitation by performing a local measurement, since the signal (the wave packet) remains local for a long time. On the other hand, in strongly interacting quantum systems, the physics of excitations is typically very different. In fact, such a system often cannot sustain any coherent excitation for very long, unless that excitation has a special reason for being protected,

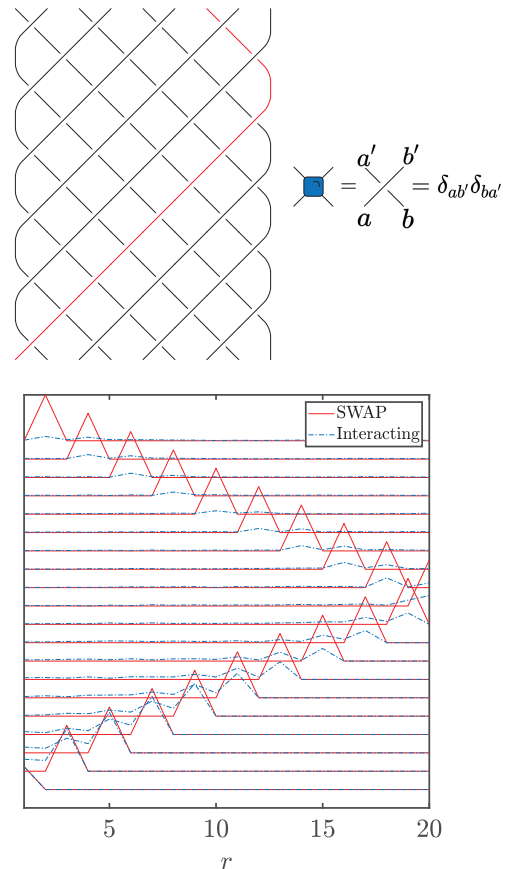


FIG. 3. (a) Quantum unitary circuit made from SWAP gate. In this case, Alice's qubit state propagates through the system coherently and remains on a single qubit (the red line). (b) The maximal signal Bob can obtain from single-qubit measurements. The x axis labels the qubit. Each line represents the signal at different time with an offset. In the case of circuits from SWAP gates (red lines), the signal remains maximal and propagates through the system. On the other hand, when we perturb the SWAP gate by multiplying it by another unitary gate close to identity, the signal decays quickly.

such as a sound mode or a Goldstone mode associated with a broken symmetry. Fig. 3 illustrates this difference between non-interacting system and strongly interacting system. We use the circuit in Fig. 3 to represent the non-interacting case, which is built from the two-qubit SWAP gate. Since the SWAP gate simply swaps the two qubits it acts on, Alice's state on the first qubit propagates coherently through the system and always remains on a single qubit which Bob can measure. On the other hand, once the local gate of the circuit is perturbed away from the SWAP gate, the signal generally decays as time increases.

The lack of the coherent excitations is a consequence of quantum thermalization. For a strongly interacting system, a time-evolved state becomes as complicated as allowed consistent with macroscopic constraints, such as

a fixed total energy. As a result, the state looks thermal locally when $t > \tau$, where τ is a relaxation time. This is to say, for any local operator O , we have

$$\langle \psi(t) | O | \psi(t) \rangle \underset{t \gg \tau}{\approx} \frac{\text{tr}(e^{-\beta H} O)}{\text{tr}(e^{-\beta H})}, \quad (14)$$

where β only depends on the average energy $\langle \psi | H | \psi \rangle$ of the initial state $|\psi\rangle$.

Let us go back to the communication protocol between Alice and Bob. Since $|\psi_0\rangle$ and $|\psi_1\rangle = \sigma_{q_A}^x |\psi_0\rangle$ only differ by a single-qubit flip, they have the same energy density. Therefore, we expect the two states to thermalize and look the same locally after a time τ . Now imagine Bob is trying to tell what Alice did by performing local measurement in a region some distance away from Alice's qubit q_A . At early time, the information lightcone has not arrived at Bob's region yet, and by definition, Bob can do nothing to tell the difference between the two states. Later, when the information lightcone reaches Bob's region, the time is well past the relaxation time τ , so Bob still cannot tell the difference since the two states since they now look the same locally. Therefore, unlike in the non-interacting case, Bob cannot tell what Alice did using only local measurements when the system thermalizes.

It is not plausible that information has simply stopped spreading in the strongly interacting system, but it becomes inaccessible to local measurements. Said differently, it may be very difficult to transmit information in the Alice-Bob communication protocol coherently. However, information is still spreading and Bob needs an approach to recover it. We know at least one approach; Bob can perform the measurement using the Heisenberg operator $\sigma_0^z(-t)$, which is highly non-local. Then it is equivalent to measuring σ^z at $t = 0$, and Bob can easily tell what Alice did. However, this approach might not be optimal since $\sigma_0^z(-t)$ can be very complex and its support contains Alice's qubit as well.

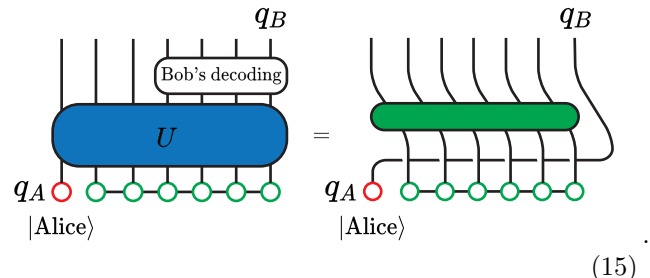
The discussion so far was framed in terms of classical information – whether Bob can tell if Alice flips her qubit or not. A stronger version is about transmitting quantum data. One can ask the following question. Given that Alice initially prepares an arbitrary quantum state on her qubit q_A , is it possible for Bob to recover that quantum state on one of his qubits, denoted q_B , following some decoding procedure, after the system is evolved by some time t ?

The takeaway of this section is that information spreading is intimately related to commutators of local operators and its speed is upper bounded by the possibly very loose Lieb-Robinson bound. This section also raises two central questions regarding quantum information dynamics in strongly interacting quantum many-body systems:

- How to detect the information propagation?
- How to recover the information?

III. QUANTUM INFORMATION FORMULATION

In this section, we formulate the general problem of information in fully quantum terms. Recall that Alice initializes one qubit, q_A , into an arbitrary quantum state. The medium that Alice and Bob share then evolves by the unitary U . Finally, Bob's goal is to apply some decoding operation to isolate the quantum information $|\text{Alice}\rangle$ that Alice originally encoded in qubit q_A ,



$$(15)$$

In general, Bob's decoding can be a very complex quantum operation. We will discuss examples of Bob's decoding in Section IV, but let's first understand how to determine which qubits Bob needs to control to decode Alice's information in principle. In other words, let's understand how to track where the quantum information is before the decoding. Remarkably, this task can be accomplished just by following a special kind of entanglement with an auxiliary reference system, as we next explain (see also Section IVB).

A. Entanglement spreading

Consider a system containing N qubits whose dynamics is described by a unitary matrix $U(t)$. We pick two orthogonal initial states, $|\psi_0\rangle$ and $|\psi_1\rangle$ that differ by a spin flip at Alice's qubit,

$$|\psi_0\rangle_{\text{SYS}} = |0\rangle_{q_A} \otimes |\psi\rangle, \quad |\psi_1\rangle_{\text{SYS}} = |1\rangle_{q_A} \otimes |\psi\rangle \quad (16)$$

where $|0\rangle$ and $|1\rangle$ are two orthogonal states in some basis on Alice's qubit q_A , and $|\psi\rangle$ is the state of the remaining system. These two states correspond to the two possible initial states in the Alice-Bob communication protocol in Sec. II.

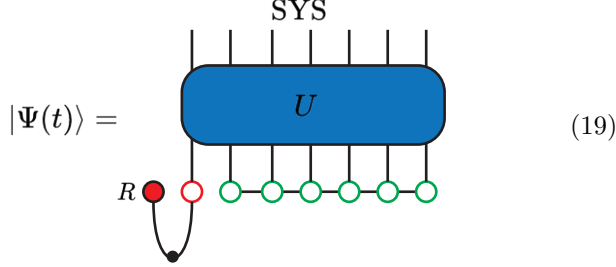
Next, introduce a new auxiliary qubit called reference R . The unitary dynamics U does not act on the reference qubit, which one may think of as sitting in an isolated box. Before isolating the reference, however, the reference qubit is entangled with the system through Alice's qubit q_A . The initial composite state of the system and the reference is

$$\begin{aligned} |\Psi\rangle &= \frac{1}{\sqrt{2}} (|0\rangle_R |\psi_0\rangle_{\text{SYS}} + |1\rangle_R |\psi_1\rangle_{\text{SYS}}) \\ &= \frac{1}{\sqrt{2}} (|0\rangle_R |0\rangle_{q_A} + |1\rangle_R |1\rangle_{q_A}) |\psi\rangle. \end{aligned} \quad (17)$$

The reference R and Alice's qubit q_A form a Bell pair and are maximally entangled. The time evolution of the state is given by

$$|\Psi(t)\rangle = \frac{1}{\sqrt{2}} (|0\rangle_R U |\psi_0\rangle_{\text{SYS}} + |1\rangle_R U |\psi_1\rangle_{\text{SYS}}) \quad (18)$$

or, graphically,



where the black dot represents the EPR state $\frac{1}{\sqrt{2}}(|00\rangle + |11\rangle)$.

This setup can be generalized to the case where the two initial states of the system are mixed. Similar to the previous case, we pick the two initial states

$$\rho_0 = |0\rangle\langle 0| \otimes \rho, \quad \rho_1 = |1\rangle\langle 1| \otimes \rho. \quad (20)$$

where ρ is the density matrix of the system, excluding the first qubit. Then we introduce the purification of the density matrix ρ by including an additional auxiliary system called memory. The purification of ρ , denoted $|\sqrt{\rho}\rangle$, is a pure state living in the Hilbert space of the system (excluding the first qubit) and the memory. It has the property that tracing out the degrees of freedom in the memory gives back the density matrix ρ ,

$$\rho = \text{tr}_{\text{MEM}} |\sqrt{\rho}\rangle\langle\sqrt{\rho}|. \quad (21)$$

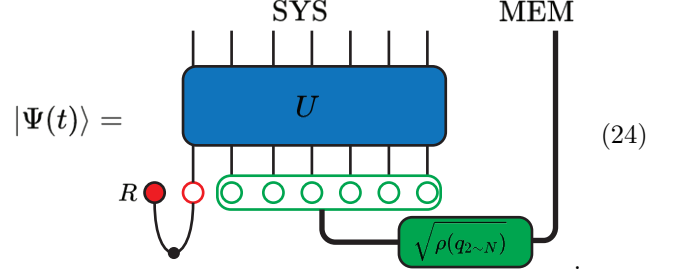
Alice's qubit still forms a Bell pair with the reference. The entire state, including the reference, the system and the memory, is

$$|\Psi\rangle = \frac{1}{\sqrt{2}} (|0\rangle_R |0\rangle_{q_A} + |1\rangle_R |1\rangle_{q_A}) |\sqrt{\rho}\rangle. \quad (22)$$

This state is very similar to Eq. (17). The difference is that $|\sqrt{\rho}\rangle$ contains degrees of freedom of the memory that the time evolution operator does not act on. The time evolution of the state is

$$|\Psi(t)\rangle = \frac{1}{\sqrt{2}} (|0\rangle_R U_{\text{SYS}} \otimes I_{\text{MEM}} |0, \sqrt{\rho}\rangle + |1\rangle_R U_{\text{SYS}} \otimes I_{\text{MEM}} |1, \sqrt{\rho}\rangle) \quad (23)$$

Graphically,



Given the initial state, we may probe the information dynamics by tracking the entanglement between the system and the reference as a function of time. Initially, the reference is only entangled with the first qubit q_A . This entanglement can be diagnosed using mutual information between R and q_A . First, define the Von Neumann entropy of a set of qubits A ,

$$S(A) = -\text{tr}(\rho_A \log_2 \rho_A) \quad (25)$$

where ρ_A is the reduced density matrix of A . Then the mutual information of A with B is

$$I(A : B) = S(A) + S(B) - S(AB) \quad (26)$$

Using subadditivity and the triangle inequality (see appendix A 2), one can show that

$$0 \leq I(A : B) \leq 2 \min(S(A), S(B)) \quad (27)$$

For R and q_A , it is straightforward to show that at $t = 0$, $S(R) = S(q_A) = 1$ and $S(R \cup q_A) = 0$ from the fact that they form a Bell pair initially. Therefore initially, $I(R : q_A) = 2$, which is the largest possible value, indicating maximal entanglement between q_A and R . Correspondingly, at $t = 0$, the mutual information between R and any other set of qubits is zero.

Starting from the initially localized entanglement, one should expect the entanglement with the reference R to expand out across the system in some fashion. One possibility is that the entanglement is carried in some coherent wavepacket throughout the system, remaining localized in space at any given time. This can occur under the right conditions in non-interacting systems, for instance, in the SWAP circuit shown in Fig. 3. However, with strong interactions, the entanglement seems likely to spread and to become more complex [17]. In other words, while at time zero the reference is entangled with one qubit, as time progresses, the reference will instead become entangled with a complex collection of many qubits. This process can be quantified by the mutual information between the reference qubit and certain regime B in the state.

For example, one can choose B to include the first l qubits $q_1 \dots q_l$ in the system. At $t = 0$, the reference is entangled with q_A contained in first l qubits. Therefore $I(R : q_1 \dots q_l) = 2$ for all l . As time increases, fixing l , $I(R : q_1 \dots q_l)$ decreases once the entanglement leaks out

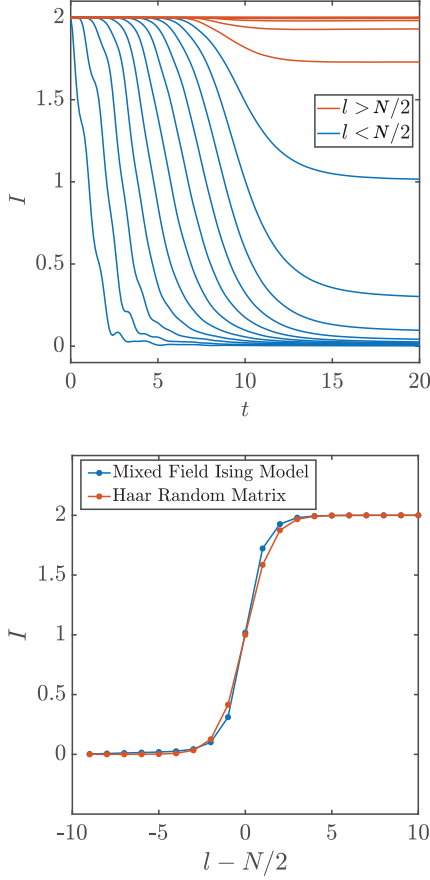


FIG. 4. (a) The mutual information between the reference qubit R and first l qubits in the system as a function of time. The parallel curves for different l is a signature of ballistic propagating quantum information. (b) The late-time value of the mutual information undergoes a sharp transition from 0 to 2 as l passes $N/2$.

the first l qubits. This behavior is illustrated in Fig. 4, where $I(R : q_1 \cdots q_l)$ for $1 \leq l \leq N$ are shown for the mixed-field Ising model containing 22 spins. Pure initial states are used here. Notice the parallel curves for $l < N/2$. This is the first concrete example of the ballistic propagation of information in a strongly interacting system in this tutorial. Also, notice that the late-time value of the mutual information increases with l and approximately stays at the maximal value of 2 for $l > N/2$. This is a signature of a strongly interacting system, which we will see again soon.

B. Alice-Bob communication again

How is entanglement spreading related to the Alice-Bob communication protocol? The description above might have already hinted at some similarities. We will now make the connection more precise. We consider a region B of the system and denote its complement as \bar{B} .

The mutual information between the reference R and B is

$$I(R : B) = S(R) + S(B) - S(RB). \quad (28)$$

which is between 0 and 2. Since the initial total state $|\Psi\rangle$ is pure, $S(RB) = S_{\bar{B}}$. Therefore

$$I(R : \bar{B}) + I(R : B) = 2. \quad (29)$$

The mutual information can also be cast into a form of relative entropy as follows,

$$I(R : B) = \text{tr}(\rho(RB) (\log \rho(RB) - \log \rho(R) \otimes \rho(B))) \quad (30)$$

Therefore $I(R : B)$ is a measure of the difference between the density matrix $\rho(R) \otimes \rho(B)$ and $\rho(RB)$. These density matrices depend on the two orthogonal states $|\psi_0\rangle$ and $|\psi_1\rangle$ used in the Alice-Bob communication protocol,

$$\begin{aligned} \rho(RB) &= \frac{1}{2} \begin{pmatrix} \rho_0(B) & \rho_{01}(B) \\ \rho_{10}(B) & \rho_1(B) \end{pmatrix}, \\ \rho(R) \otimes \rho(B) &= \frac{1}{4} \begin{pmatrix} \rho_0(B) + \rho_1(B) & 0 \\ 0 & \rho_0(B) + \rho_1(B) \end{pmatrix} \end{aligned} \quad (31)$$

where

$$\begin{aligned} \rho_0(B) &= \text{tr}_B |\psi_0\rangle \langle \psi_0|, \quad \rho_1(B) = \text{tr}_B |\psi_1\rangle \langle \psi_1| \\ \rho_{01}(B) &= \rho_{01}(B)^\dagger = \text{tr}_B |\psi_0\rangle \langle \psi_1| \end{aligned} \quad (32)$$

Now we discuss the implication of the minimum and maximum of $I(R : B)$ on the Alice-Bob communication protocol. From the quantum relative entropy, $I(R : B)$ is zero only when $\rho_{RB} = \rho_R \otimes \rho_B$, leading to the condition $\rho_0(B) = \rho_1(B)$ and $\rho_{01}(B) = 0$. As a result

$$\langle \psi_1 | O_B | \psi_1 \rangle = \langle \psi_0 | O_B | \psi_0 \rangle, \quad \langle \psi_1 | O_B | \psi_0 \rangle = 0 \quad (33)$$

for arbitrary operator O_B within region B , indicating no operators in B can distinguish the two state. To make the implication of these conditions on the state $|\psi_0\rangle$ and $|\psi_1\rangle$ manifest, we perform a singular value decomposition on both states between regime B and \bar{B} ,

$$|\psi_0\rangle = \sum_n \lambda_0^{(n)} |\psi_0^{n,B}\rangle |\psi_0^{n,\bar{B}}\rangle, \quad |\psi_1\rangle = \sum_n \lambda_1^{(n)} |\psi_1^{n,B}\rangle |\psi_1^{n,\bar{B}}\rangle. \quad (34)$$

The conditions $\rho_0(B) = \rho_1(B)$ and $\rho_{01}(B) = 0$ are equivalent to

$$\lambda_0^{(n)} = \lambda_1^{(n)}, \quad \langle \psi_0^{n,B} | \psi_1^{m,B} \rangle = \delta_{mn}, \quad \langle \psi_0^{n,\bar{B}} | \psi_1^{m,\bar{B}} \rangle = 0. \quad (35)$$

An arbitrary superposition of $|\psi_0\rangle$ and $|\psi_1\rangle$ has the same density matrix in the region B and thus is the same to Bob.

In the opposite limit, $I(R : B)$ takes the maximal value 2 if and only if $I(R : \bar{B}) = 0$. This leads to the same condition in Eq. (34) with B replaced with \bar{B} . As a result, $\rho_0(B) = \sum_n \lambda^{(n),2} |\psi_0^{n,B}\rangle \langle \psi_0^{n,B}|$ and

$\rho_1(B) = \sum_n \lambda^{(n),2} |\psi_1^{n,B}\rangle \langle \psi_1^{n,B}|$ act on orthogonal states in the Hilbert space of B , and $|\rho_1(B) - \rho_0(B)| = 2$, indicating maximal difference between the two states in region B . In this case, in principle, the optimal operator O_B that differentiates the two states can be constructed as

$$O_B = \sum_n |\psi_0^{n,B}\rangle \langle \psi_0^{n,B}| - |\psi_1^{n,B}\rangle \langle \psi_1^{n,B}| \quad (36)$$

so that $\langle \psi_0 | O_B | \psi_0 \rangle = 1$ and $\langle \psi_1 | O_B | \psi_1 \rangle = -1$.

What happens when $I(R : B)$ is small but finite? By the quantum Pinsker's inequality, we have,

$$I(R : B) \geq \frac{1}{2 \ln 2} \text{tr} |\rho(RB) - \rho(R) \otimes \rho(B)|^2. \quad (37)$$

This can be further applied to upper bound any connected correlation between R and A ,

$$I(R : B) \geq \frac{(\langle O_R O_B \rangle - \langle O_R \rangle \langle O_B \rangle)^2}{2 \|O_R\|_\infty^2 \|O_B\|_\infty^2} \quad (38)$$

Applying this inequality to all Pauli operators O_R , leading to

$$\begin{aligned} \frac{1}{\|O_B\|_\infty} |\langle \psi_0 | O_B | \psi_0 \rangle - \langle \psi_1 | O_B | \psi_1 \rangle| &\leq \sqrt{2 \ln 2 I(R : B)} \\ \frac{1}{\|O_B\|_\infty} |\langle \psi_0 | O_B | \psi_1 \rangle| &\leq \sqrt{2 \ln 2 I(R : B)} \end{aligned} \quad (39)$$

Therefore, the smallness of $I(R : B)$ prevents Bob from distinguishing the two states.

C. Quantum mutual information from random unitary dynamics

As we have seen from comparing the non-interacting (Fig. 3) and strongly interacting (Fig. 4) cases, the quantum mutual information between the reference R and a certain region of the system B $I(R : B)$ depends on the unitary operator U that governs the dynamics. To gain intuition for I in a strongly interacting system, we next consider a simple toy model where U is taken to be a random unitary operator drawn from the Haar measure.

It is important to understand that a random unitary matrix is a generic matrix acting on the Hilbert space where the states live and does not obey a local structure sketched in Fig. 2. Nevertheless, random unitary dynamics is a good starting point to think about quantum information dynamics. It can be used to mimic the local unitary dynamics in the late time regime where the initial entanglement between the reference and the system is fully scrambled over all degrees of freedom.

To proceed, we consider the Rényi version of the mutual information,

$$I^{(2)}(R : B) = S^{(2)}(R) + S^{(2)}(B) - S^{(2)}(RB) \quad (40)$$

where $S^{(2)}$ stands for the Rényi entropy. We start with the case without the memory, where the combined state of the reference R and system is pure. Recall that the time evolved state is given in Eq. (18),

$$|\Psi(t)\rangle = \frac{1}{\sqrt{2}} (|0\rangle_R U_{\text{Haar}} |\psi_1\rangle_{\text{SYS}} + |1\rangle_R U_{\text{Haar}} |\psi_0\rangle_{\text{SYS}})$$

Of course, the Rényi entropy of any particular U is in principle a complicated function of U , but what is analytically tractable is an average of the Rényi entropy over all U sampled from Haar measure. The averaged Rényi entropy captures well the Rényi entropy of a particular U for large systems because the variance is strongly suppressed by the system size.

The Rényi entropy averaged over Haar random unitaries can be calculated using the identities in Eq. (A9). We have,

$$\begin{aligned} 2^{-S(B)} &= \mathbb{E} \left(\text{tr}_B (\text{tr}_{R\bar{B}} |\Psi\rangle \langle \Psi|)^2 \right) \\ &= \frac{1}{2^{2N} - 1} \left(\left(\frac{1}{2} - \frac{1}{2^N} \right) 2^{N+l} + \left(1 - \frac{1}{2^{N+l}} \right) 2^{2N-l} \right) \\ &\approx \left(\frac{1}{2} - \frac{1}{2^N} \right) 2^{l-N-1} + 2^{-l} \end{aligned} \quad (41)$$

Since there is no notion of locality associated with U_{Haar} , the results only depend on the size l of the region B but not its location in the system. We have taken the limit that $N \rightarrow \infty$ in the last line. The entropy $S(RB)$ is the same as that of the complement of B $S(\bar{B})$ and can be obtained by replace l with $N - l$ in $S(B)$.

Putting these results together, we obtain the Rényi mutual information as

$$I^{(2)}(l) = 1 + \log_2 \left(2 - \frac{3(1 - 2^{2l-2N})}{2 + 4^{l-N/2}} \right) \quad (42)$$

The mutual information is 1 when $l = N/2$, i.e., the region B occupies half the system. It increases to its maximal value of 2 as l exceeds $N/2$ and decreases to its minimal value of 0 exponentially when l is less than $N/2$. This result indicates that when the initial information is fully scrambled, any portion of the system less than half does not contain the initial information. On the other hand, any portion larger than half is maximally entangled with the reference spin R and can be used to recover the initial information. This is in sharp contrast with the non-scrambling SWAP circuit shown in Fig. 3 where the information is located at a specific qubit at a given time.

The change of the mutual information at $l = N/2$ can be understood as follows. The system contains two disconnected regions with $l < N/2$, but the reference spin cannot be simultaneously maximally entangled with two non-overlapping regions, otherwise it would violate the monogamy of entanglement. As a result, the mutual information drastically reduces when $l < N/2$.

This result is also valid in the late time regime of local unitary dynamics or even Hamiltonian dynamics. As

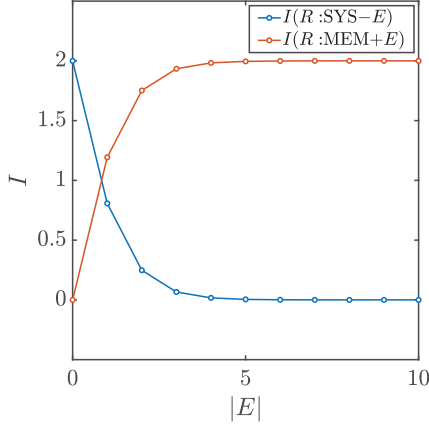


FIG. 5. In fully mixed initial state setup, after applying the Haar random unitary to the system, the mutual information between the reference and the system excluding a few qubits decays exponentially with the number of qubits excluded. On the contrary, the mutual information between the reference and the memory plus a few qubits in the system saturates to the maximum.

shown in Fig. 5, for the mixed-field Ising model, the late time value of mutual information for different regions obeys the random unitary calculation, drastically increasing from 0 to 2 when the region considered exceeds half of the system. In the large N limit, I increases from 0.033 to 1.967 in a window of 6 qubits around $N/2$.

Now we consider another case where the initial state on the system (excluding the first spin) is mixed. The mixed state can be viewed as a result of entanglement between the system and the memory. Initially the first spin is still maximally entangled with the reference. The time evolved state including the reference, the system and the memory is given in Eq. (23),

$$|\Psi(t)\rangle = \frac{1}{\sqrt{2}} (|0\rangle_R U_{\text{SYS}} \otimes I_{\text{MEM}} |0, \sqrt{\rho}\rangle + |1\rangle_R U_{\text{SYS}} \otimes I_{\text{MEM}} |1, \sqrt{\rho}\rangle)$$

A similar calculation of the averaged Rényi entropy now yields

$$\begin{aligned} 2^{-S_B} &\approx \left(\frac{\text{tr} \rho^2}{2} - \frac{1}{2^N} \right) 2^{l-N} + 2^{-l}, \\ 2^{-S_{RB}} &\approx \left(\text{tr} \rho^2 - \frac{1}{2^{N+1}} \right) 2^{l-N} + 2^{-l-1}. \end{aligned} \quad (43)$$

Therefore the mutual information is

$$I^{(2)}(l) = 1 + \log_2 \left(2 - \frac{3(1 - 2^{2l-2N})}{2 + (2^{-s} - 2^{-N+1})4^{l-N/2}} \right) \quad (44)$$

where $s(\rho)$ is the Rényi entropy of ρ in the initial state. It reduces back to Eq. (42) when the initial state is pure, i.e. $s = 0$. When the initial state is mixed and has finite entropy, $I(l)$ drastically increases from 0 to its maximal

value 2 at $l \sim (N + s)/2$. The behavior of $I(l)$ for l near $(N + s)/2$ is independent of s in the large N limit and is already shown in Fig. 5. This result suggests that one now needs more than $(N + s)/2$ qubits to recover the initial information.

In the special case when the initial state is maximally mixed, $s(\rho) = N - 1$ (the first spin is entangled with the reference spin). In this case, $I = \log_2(1 + 3 \times 2^{2l-2N})$ and equals 2 when $l = N$, i.e. the entire system. $I^{(2)}$ drastically decreases as the accessible region contains fewer qubits. These results also apply to the late time regime of unitary dynamics. Denote the part of the system that Bob does not have access to as E , and the number of qubits in this region as $|E|$. We have

$$I^{(2)}(R : \text{SYS} - E) = \log_2(1 + 3 \times 4^{-|E|}). \quad (45)$$

This behavior is plotted in Fig. 5.

In this special case, the Rényi mutual information can be used to bound the Von Neumann entropy because the Rényi entropy $S^{(2)}(\text{SYS} - E)$ and $S^{(2)}(R)$ are maximal and equal their Von Neumann counterpart. Since $S^{(2)}(R \cup (\text{SYS} - E)) \leq S(R \cup (\text{SYS} - E))$, we have

$$\begin{aligned} I(R : \text{SYS} - E) &\leq I^{(2)}(R : \text{SYS} - E) \\ &= \log_2(1 + 3 \times 4^{-|E|}) \end{aligned} \quad (46)$$

Combining with $I(R : \text{SYS}) = 2$, this indicates that recovering the initial information requires accessing the entire system when the initial state is maximally mixed, in contrast with half of the system for pure initial state.

Another closely related diagnosis of scrambling in this special setup is the tripartite mutual information [12, 18] given by

$$\begin{aligned} I_3(R : E : \text{SYS} - E) \\ = I(R : E) + I(R : \text{SYS} - E) - I(R : \text{SYS}) \end{aligned} \quad (47)$$

which quantifies how much information is not encoded in E and $\text{SYS} - E$ but in their composite.

IV. HAYDEN-PRESKILL PROTOCOL: DETECTING AND RECOVERING THE INFORMATION

Having understood where the information is located at late time, let us now understand how to recover the information. We start with the fully mixed case as this was the setup first studied in the Hayden-Preskill protocol [7], which was originally proposed for black hole dynamics. In the black hole problem, the memory is supposed to describe previously emitted Hawking radiation which is entangled with the remaining black hole. The maximally mixed case then corresponds to the entropic midpoint of the black hole's evolution. The question posed in Ref. [7] was: if another qubit is thrown into the black hole, then how long does one have to wait until the information

in that qubit is available again in the subsequent radiation. The result of the prior section is that when Bob has access to the memory (the early radiation), then the information in the fresh qubit quickly becomes available again.

As shown in Fig. 5(b), when the accessible region of Bob is $\text{SYS} - E$ drastically reduces to zero as the number of qubits in E increases. Then Bob needs the entire system to recover the information. What happens when Bob also has access to the qubits in the memory? The memory is only coupled to the system by the initial entanglement, the unitary dynamics never mixing the system and memory. As a result, one expects that the memory does not contain any information about the reference, indicated by zero mutual information. On the other hand, since quantum state on the composite system include the reference, system and memory is pure, we have

$$I(R : \text{SYS} - E) + I(R : \text{MEM} + E) = 2. \quad (48)$$

Thus according to Eq. (46),

$$I(R : \text{MEM} + E) \geq 2 - \log_2(1 + 3 \times 4^{-|E|}). \quad (49)$$

$I(R : \text{MEM} + E)$ saturates to the maximal value 2 exponentially fast, shown in Fig. 5(b). In other words, remarkably, Bob can recover the initial information provided that he has access to the full memory, which does not contain any information about the reference, and a few qubits E in the system.

A. Detecting the information front

The Hayden-Preskill protocol also provides an operational way to measure the information dynamics. Let us still consider the setup with fully mixed initial state. The unitary operator U governing the dynamics now may have more structure, such as locality, instead of being Haar random. Under time evolution, the mutual information between the reference R and the system SYS is always maximal, and the mutual information between the reference and the MEM is always 0. Initially, R is maximally entangled with the first spin. As discussed previously, when the unitary operator is Haar random, the entanglement instantly spreads over the entire system. The mutual information between the reference to any subregion of the output, even excluding a few qubits, becomes almost 0.

Now suppose the unitary operator has a local structure built in, so that the entanglement spreads in a time-dependent manner, as shown in Fig. 4. In order to capture the profile of the entanglement spreading, a natural approach is to trace the mutual information between the reference and the first l qubits in the output $I(R : q_{1 \sim l})$, which increases monotonically with l . The front of the spreading at a given time is determined by the largest l for which $I(R : q_1 \cdots q_n) < 2$, because it implies that the information has begun to leak out the first l qubits.

This approach is a conceptually straightforward application of the definition, but is challenging for experiments since $I(R : q_1 \cdots q_n)$ involves the entanglement entropy of a nonlocal region. Alternatively, inspired by Hayden-Preskill, one can measure the mutual information between the reference and the memory plus one qubit in the system $I(R : \text{MEM} \cup q_n)$. A finite value indicates that the initial information has reached the l th spin. Therefore the front of the entanglement spreading can be determined by the largest n that $I(R : \text{MEM} \cup q_n) > 0$.

The mutual information used in the second approach can be estimated by local measurement, as we discuss below, and is much more accessible in experiments. Now let us look into the mutual information $I(R : \text{MEM} \cup q_n)$ more closely. From the definition of I , we have

$$\begin{aligned} I(R : \text{MEM} \cup q_n) &= S(R) + S(\text{MEM} \cup q_n) - S(R \cup \text{MEM} \cup q_n) \\ &= S(R) + S(\text{MEM} \cup q_n) - S(\text{SYS} - q_n) \end{aligned} \quad (50)$$

In the second equality, we used the fact that $R \cup \text{MEM} \cup q_n$ and $\text{SYS} - q_n$ are complementary regions in a pure state. Because the fully mixed state is used in the setup, $S(R) = 1$ and $S(\text{SYS} - q_n) = N - 1$. Therefore the mutual information only depends the entanglement entropy of $B \cup q_n$,

$$\begin{aligned} I(R : \text{MEM} \cup q_n) &= 2 - N + S(\text{MEM} \cup q_n) \\ N - 2 &\leq S(\text{MEM} \cup q_n) \leq N. \end{aligned} \quad (51)$$

Initially, $S(\text{MEM} \cup q_n)$ takes the minimal value for all qubits q_n except the first one. As time increases, its deviation away from the minimal value signals that the information has reached the n th spin. Since the Von Neumann entropy upper bounds the Rényi entropy, we have,

$$I(R : \text{MEM} \cup q_n) \geq 2 - N + S^{(2)}(\text{MEM} \cup q_n) \quad (52)$$

As a result, $S^{(2)}$ can be used as an indicator for the front of quantum information propagator. This result is particularly nice, since $S^{(2)}$ can be related to correlation functions that are more accessible than the von Neumann mutual information, as we shown below. Also see experimental scheme in Sec. VIII.

Since in the case we consider here, the qubits $q_{2 \sim N}$ are in a fully mixed state, we can choose the simplest purification where the memory contains $N - 1$ auxiliary qubits that form $N - 1$ EPR pairs with the $N - 1$ spins in the system. The time evolved state and the density

matrix $\rho(\text{MEM} \cup q_n)$ is

$$|\Psi(t)\rangle = \text{Circuit with inputs } R, q_n, \text{MEM \text{ and unitary } U.}$$

$$\rho(\text{MEM} \cup q_n) = \frac{1}{2} \text{Circuit with inputs } q_1, q_n \text{ and unitaries } U, U^\dagger. \quad (53)$$

From the density matrix, we can obtain the purity $\text{tr}(\rho^2(\text{MEM} \cup q_n)) = e^{-S^{(2)}(\text{MEM} \cup q_n)}$ as

$$\text{tr}(\rho^2(\text{MEM} \cup q_n)) = \frac{1}{4^N} \text{Circuit with } U, U^\dagger.$$

$$= \frac{1}{4^{N+1}} \sum_{W,V} \text{Circuit with } U, U^\dagger, V, W. \quad (54)$$

The operators V and W are summed over local Pauli operators (including the identity) on q_1 and q_n . In the

last line we have used the completeness relation of Pauli operators. When either V_1 or W_n equals the identity, the trace contributes 1 to the sum. Separating these terms from the others, we get,

$$\text{tr} \rho^2(\text{MEM} \cup q_n) = \frac{1}{2^{N+2}} \left(7 + \sum_{\substack{W_1 \neq I \\ V_n \neq I}} \frac{1}{2^N} \text{tr}(W_1(-t)V_n W_1(-t)V_n) \right) \quad (55)$$

The purity becomes a sum of local correlators between Pauli operators. The Rényi entropy is just $-\log_2 \text{tr}(\rho^2)$. From Eq. (55), we can bound the mutual information by the correlators,

$$I(R : \text{MEM} \cup q_n) \geq 4 - \log_2 \left(7 + \sum_{\substack{V_1 \neq I \\ W_n \neq I}} \frac{1}{2^N} \text{tr}(W_1(-t)V_n W_1(-t)V_n) \right). \quad (56)$$

We emphasize that this inequality applies to any unitary U . Each term in the summation has maximum value 1, in which case the right-hand side takes the minimal value 0. This happens when the Heisenberg operator $V_1(-t)$ commutes with the operator W_n for all V and W . When $V_1(-t)$ and W_n start to overlap, the correlator decreases from 1. As a result, $I(R : \text{MEM} \cup q_n)$ is nonzero, indicating that the information has reached q_n . At late time, all the terms decays to 0 and the right hand side becomes $4 - \log_2 7$, consistent with Eq. (49) when $|E| = 1$.

Because the kind of correlator appearing on the right-hand side of Eq. (56) can be used to diagnose the information propagation, it deserves a name. In the literature, it is referred to as the out-of-time ordered correlator or OTOC, usually written as

$$F(t) = \frac{1}{2^N} \text{tr}(W_1(t)V_n W_1(t)V_n). \quad (57)$$

OTOC was first introduced by Larkin and Ovchinnikov in the context of superconductivity [19], and have gained extensive renewed interests recently due to the connection to scrambling dynamics discussed here as well as quantum many-body chaos in the semi-classical regime.

Several remarks are in order. First, we emphasize that the OTOC is only an indicator of information propagation and scrambling. Nonzero squared commutator between $W_1(t)$ and V_n only indicates that the information front has reached qubit n , and does not mean that one can recover Alice's initial action by measuring the n th qubit. In fact, we have seen from the random unitary calculation that it requires all qubits with nonzero squared commutator, or the entire memory plus a few qubits with nonzero commutators, to recover the information. Second, the squared commutator as an indicator of the information propagation is tied to the simple initial state

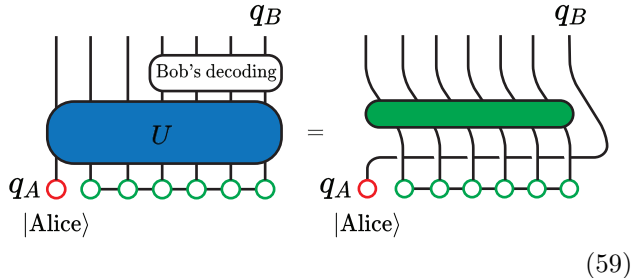
where $\rho(q_2 \sim N)$ is fully mixed. When the initial state is not fully mixed, a precise relation between the mutual information, which is the defining characterization of information propagation, and simple correlations functions such as OTOC is not established. One can even show that the OTOC overestimates how fast information propagates for some other initial states.

B. Recovering the information: many-body teleportation

This section discusses the second question of quantum information dynamics on how to recover the initial information. In Sec. III B, we showed that maximal mutual information between the reference and Bob's qubits indicates that Bob can distinguish Alice's action on the initial state using the operator constructed in Eq. (36). However, in practice, the optimal operator O_B is nonlocal and challenging to construct. It will be ideal if the initial state of Alice's qubit q_A reappears on one of Bob's qubits after Bob follows a specific decoding protocol on his qubits. This is called many-body teleportation [7, 20–22]. Many-body teleportation works if

$$U(|\text{Alice}\rangle_{q_A} \otimes |\psi\rangle) \xrightarrow{\text{Bob's decoding}} |\phi\rangle \otimes |\text{Alice}\rangle_{q_B} \quad (58)$$

for any state $|\text{Alice}\rangle$ to be teleported, where q_A is Alice's qubit, q_B is one of Bob's qubit, $|\psi\rangle$ is the initial state on the qubits except q_A and $|\phi\rangle$ is the final state on the qubits except q_B . This means that Alice would be able to teleport a bit of quantum information to Bob through a strongly interacting medium described by U , which fully scrambles her information into the entire system. The key point here is that Bob only owns part of the qubits so he cannot trivially unscramble the information by applying U^\dagger . Graphically, the condition for successful teleportation is



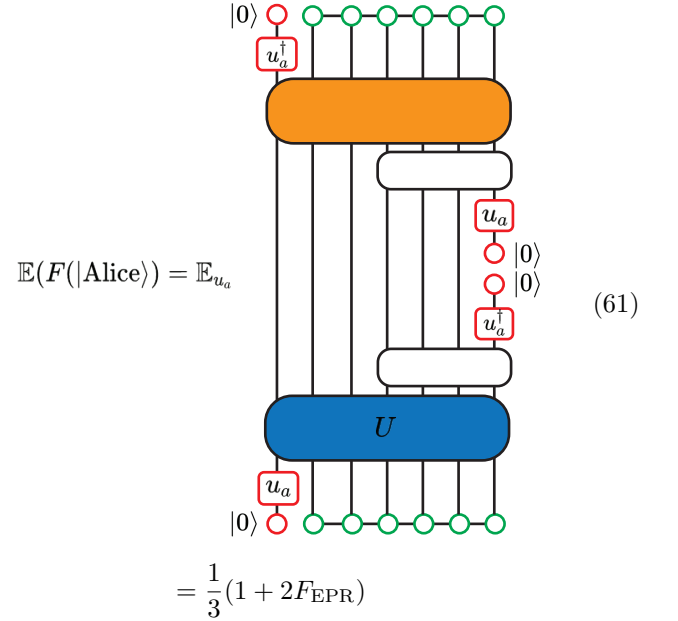
$$(59)$$

Denote the quantum state after the decoding $|\Psi_{\text{out}}\rangle$, the fidelity of teleporting the state $|\text{Alice}\rangle$ to the qubit q_B is defined as

$$F(|\text{Alice}\rangle) = \langle \Psi_{\text{out}} | (|\text{Alice}\rangle \langle \text{Alice}|)_{q_B} \otimes I | \Psi_{\text{out}} \rangle. \quad (60)$$

When the fidelity averaged over Alice's state $\mathbb{E}(F(|\text{Alice}\rangle))$ is 1, it indicates that the system is able to teleport any quantum state with perfect fidelity. The averaged fidelity can be obtained by sampling

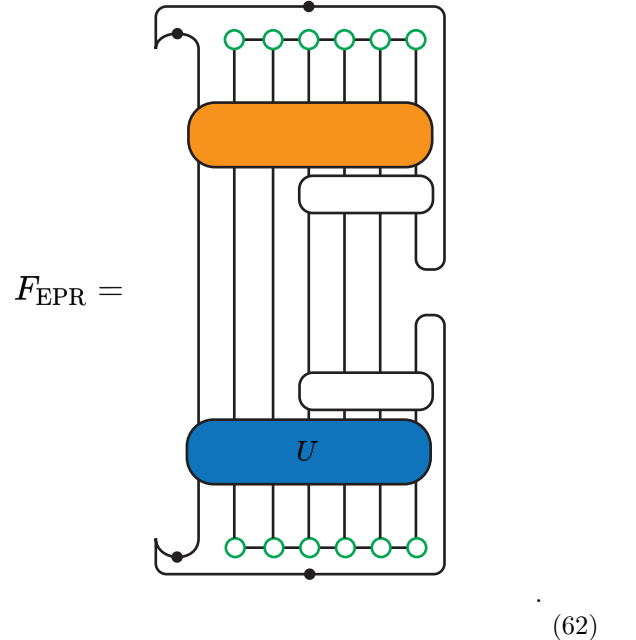
Alice's state from the action of a random unitary u_a on a basis state $|0\rangle$,



$$\mathbb{E}(F(|\text{Alice}\rangle)) = \mathbb{E}_{u_a} \quad (61)$$

$$= \frac{1}{3}(1 + 2F_{\text{EPR}})$$

where



$$F_{\text{EPR}} = \quad (62)$$

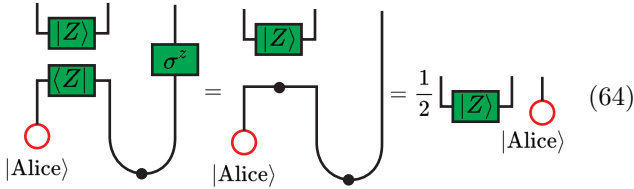
Recall the setup with the reference R used in Eq. (18) and (23). F_{EPR} is just the fidelity that the reference R , initially forming an EPR pair with Alice's qubit q_1 , forms an EPR with one of Bob's qubits after the unitary transformation and decoding. $F_{\text{EPR}} = 1$ indicates perfect teleportation. In this case, the mutual information between the reference and Bob's qubit q_B is 2. The necessary condition for the perfect teleportation is that the reference and all of Bob's qubits $I(R : B)$ is 2, as discussed in Sec. III. The purpose of the decoder is to concentrate the entanglement with the reference to a single qubit q_B .

Even given maximal mutual information $I(R : B)$, it is still in general challenging to design the decoding protocol.

Before discussing the decoder for the Hayden-Preskill protocol, it is useful to review conventional quantum teleportation. Alice has a qubit encoding the state to be teleported $|\text{Alice}\rangle$. Alice has an additional qubit that forms an EPR state with Bob's qubit. To teleport the state $|\text{Alice}\rangle$ to Bob's qubit, Alice first measures her two qubits in the Bell basis. The measurement projects the two qubits into one of the four Bell states,

$$\begin{aligned} |I\rangle &= \frac{1}{\sqrt{2}}(|00\rangle + |11\rangle) & |X\rangle &= \frac{1}{\sqrt{2}}(|01\rangle + |10\rangle) \\ |Y\rangle &= \frac{1}{\sqrt{2}}(|01\rangle - |10\rangle) & |Z\rangle &= \frac{1}{\sqrt{2}}(|00\rangle - |11\rangle) \end{aligned} \quad (63)$$

Those states obey that $I \otimes \sigma^x |X\rangle = I \otimes \sigma^y |Y\rangle = I \otimes \sigma^z |Z\rangle = |I\rangle$. After the measurement, Alice tells Bob the Bell state $|s\rangle$ she obtained. Based on Alice's message, Bob applies the corresponding Pauli operator to his qubit or does nothing if the Bell state is $|I\rangle$. Then the state $|\text{Alice}\rangle$ appears on Bob's qubit. To see why it works, we can visualize the final state of Alice and Bob for a specific outcome of the Bell measurement,

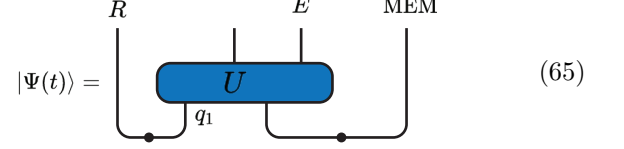


$$= \frac{1}{2} |\text{Alice}\rangle \quad (64)$$

where the coefficient $1/2$ is the square root of the probability of this Bell measurement outcome. Changing $|Z\rangle$ and σ_z for the other three outcomes, we obtain the similar final states. The probability for all the four measurement outcomes is $1/4$, and in all cases, the state $|\text{Alice}\rangle$ appears on Bob's qubit with perfect fidelity. Taken all the four measurement outcomes into account, the final state is a mixed state $\frac{1}{4} I_{\text{Alice}} |\text{Alice}\rangle_{\text{Bob}} \langle \text{Alice}|_{\text{Bob}}$, in which Alice's two qubits are in the fully mixed state and Bob has Alice's original state. One can also show that if we introduce an additional reference qubit forming an EPR with Alice's first qubit and perform the same protocol, the reference will form an EPR with Bob's qubit in the final state with fidelity $F_{\text{EPR}} = 1$.

Now we are ready to discuss the decoding protocol for the Hayden-Preskill protocol [20]. Recall the setup for the Hayden-Preskill protocol. The system contains N qubits. The first one forms an EPR with the reference R , the remaining $N - 1$ qubits form $N - 1$ EPR with another $N - 1$ auxiliary qubits in the memory, which Bob owns. In addition, Bob owns a set of qubits E in the system as well. In the Sec. IV, we showed that $I(R : B)$ approaches 2 exponentially fast as $|E|$ increases when the system is time evolved into the late-time regime and fully scrambled, therefore a decoding protocol is in principle

possible. The question now is how to design a decoding protocol on Bob's protocol so that R forms an EPR with one of Bob's qubits. The quality of the decoding protocol can be characterized by F_{EPR} . The state before the decoding is

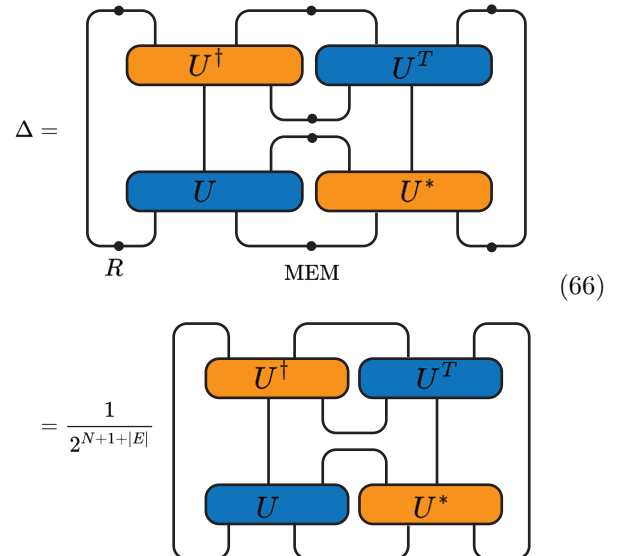


$$|\Psi(t)\rangle = \quad (65)$$

Yoshida and Kitaev [20] found two decoding protocols for this state, one probabilistic and one deterministic. The probabilistic decoding protocol goes as follows.

1. Bob takes another two qubits, q'_1 and R' and prepares them in a EPR state.
2. Bob applies the unitary operator U^* to $\text{MEM} \cup q'_1$.
3. Bob performs Bell's measurement on each qubit in E and its partner in MEM, with which it forms an EPR initially.
4. The entire protocol is repeated including preparing the state in Eq. (65) until the outcome of all the Bell measurement is the EPR state $|I\rangle$.

After these steps, the reference R and R' , one of Bob's new qubits, would have high fidelity to form an EPR. This implies that in the case without the reference, any state injected into q_1 initially has a high fidelity to reappear on R' , the other Bob's new qubit. This protocol is probabilistic because in step 3 Bob needs to postselect the EPR pairs from the Bell measurements. To understand this decoder, let us calculate the probability of successful postselection and the fidelity $F_{\text{EPR}}(R, R')$ given successful postselection. The probability of successful postselection is



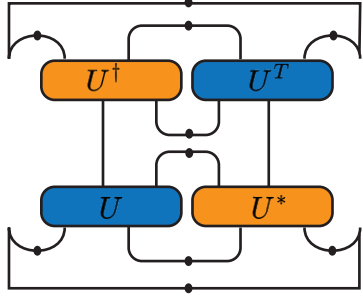
$$\Delta = \quad (66)$$

$$= \frac{1}{2^{N+1+|E|}}$$

Notice that the diagram is the same as that in Eq. (54) for calculating $\rho^2(\text{MEM} \cup E)$. Using $S^{(2)}(R) = 1$ and $S^{(2)}(R \cup \text{MEM} \cup E) = N - |E|$, we have

$$\Delta = 2^{N-1-E} \text{tr}^2(\rho_{\text{MEM} \cup E}) = 2^{-I^{(2)}(R:\text{MEM} \cup E)} \quad (67)$$

The probability of the postselection is directly related to the Rényi mutual information between R and Bob's qubit before the decoding. Given the successful postselection, the fidelity that R and R' form an EPR is



$$F_{\text{EPR}} = \frac{1}{4\Delta} = 2^{I^{(2)}(R:\text{MEM} \cup E) - 2} \quad (68)$$

When the unitary U is fully scrambling, such as a Haar random unitary, the Rényi mutual information can be obtained from Eq. (45) as

$$\begin{aligned} I^{(2)}(R : \text{MEM} \cup E) &= 2 - I^{(2)}(R : \text{SYS} - E) \\ &= 2 - \log_2(1 + 3 \times 4^{-|E|}). \end{aligned} \quad (69)$$

Substituting it in the equation for F_{EPR} , we get

$$F_{\text{EPR}} = \frac{1}{1 + 3 \times 4^{-|E|}} \quad (70)$$

F_{EPR} approaches 1 exponentially fast as $|E|$ increases, indicating perfect teleportation fidelity given successful postselection for fully scrambling unitary time evolution. In general, since $\text{tr}^2 \rho^2(\text{MEM} \cup E)$ can be written as the sum of OTOCs as shown in Eq. (54), the fidelity F_{EPR} is also directly related to OTOCs as

$$F_{\text{EPR}} = \left(\frac{1}{4^{|E|}} \frac{1}{2^N} \sum_{W_1, V_E} \text{tr}(W_1(-t) V_E W_1(-t) V_E) \right)^{-1} \quad (71)$$

where V_1 and W_E are summed over all local operators, including the identity, in the first qubit and E , respectively. In the fully scrambled regime, the OTOC is 1 if either V_1 or W_E is the identity and 0 otherwise, and we get Eq. (70) back. We see that OTOC not only provides a tool to detect the information propagation, but is also directly related to fidelity of information recovering.

The above decoding protocol is probabilistic. Bob has to postselect the state on $E \cup E'$ to be the EPR state after the Bell measurement. The probability Δ is directly related to the Rényi mutual information between

the reference and Bob, $\Delta = 2^{-I^{(2)}(R:\text{MEM} \cup E)}$. The optimal fidelity F_{EPR} requires the minimal Δ , which is $1/4$ for teleporting single qubit and 4^{-n} for teleporting multiple qubits. To overcome the small successful postselection probability, Yoshida and Kitaev [20] also designed a deterministic decoder that does not require postselection but only unitary transformation on Bob's qubits. The general idea is to perform a Grover search on Bob's qubits. After a series of unitary transformation, the states in which E does not form EPR with E' is cancelled due to destructive interference.

The above discussion assumes that the reference, system and the memory form a closed system and the dynamics is unitary. It would also be interesting to study how dissipation and measurement affect the recovery fidelity [23, 24].

V. MICROSCOPIC PHYSICS OF OPERATOR GROWTH

A. Relating OTOC to operator dynamics

In previous sections, we established that OTOCs can be used to track the front of the information dynamics, and they are directly related to the fidelity to recover the initial information. In this section, we discuss the microscopic physics of OTOCs in terms of the growth of Heisenberg operators [25, 26].

We consider a quantum many-body system whose dynamics are governed by a unitary operator $U(t)$. We use $W(t) = U^\dagger(t) W U$ to represent the time evolved Heisenberg operator, which is located at the origin at $t = 0$, and use V_r as a static local operator at site r . Then the OTOC between $W(t)$ and V_r can be written as

$$F(r, t) = \frac{1}{\text{tr} I} \text{tr}(W^\dagger(t) V_r^\dagger W(t) V_r). \quad (72)$$

The space and time dependence of $F(r, t)$ has a very intuitive picture based on operator growth, sensitive to whether the support of $W(t)$ overlaps with that of V_r . The connection between OTOC and operator growth can be made more explicit by introducing the squared commutator

$$C(r, t) = \frac{1}{\text{tr} I} \text{tr}([W(t), V_r]^\dagger [W(t), V_r]) = \frac{1}{\text{tr} I} \| [W(t), V_r] \|_2^2 \quad (73)$$

which is proportional to the Frobenius norm of the commutator $[W(t), V_r]$ and thus always positive. One can easily show that

$$\begin{aligned} C(r, t) &= -F(r, t) - F^*(r, t) \\ &\quad + \frac{1}{\text{tr} I} (\text{tr}(W^\dagger(t) V_r^\dagger V_r W(t)) + \text{tr}(V_r^\dagger W^\dagger(t) W(t) V_r)) \end{aligned} \quad (74)$$

The last two terms are local observables that typically relax to a constant in a short time due to thermalization.

Therefore, $C(r, t)$ and $F(r, t)$ have the same behavior after a thermalization time. In particular, if both W and V are unitary, the sum of the last two terms is simply 2. Furthermore, when W and V are Hermitian, $F(r, t)$ is real. Therefore, when W and V are unitary and Hermitian, e.g., Pauli operators, $C(r, t) = 2 - 2F(r, t)$.

The squared commutator manifestly depends on the “size” of the Heisenberg operator $W(t)$, the number of degrees of freedom that $W(t)$ acts on. At $t = 0$, $W(t)$ only acts on a simple site and commutes with any V_r that is far away, so $C(r, t) = 0$. (In a fermionic system, if the operator W and V are both fermionic, one should consider a squared anti-commutator instead of a squared commutator.) As time increases, $W(t)$ becomes more and more non-local and starts to overlap with V_r , indicated by the increase of $C(r, t)$. Varying V_r for different r , $C(r, t)$ remains small if V_r is outside the support of $W(t)$ and large otherwise. Therefore $C(r, t)$ probes the size of the Heisenberg operator $W(t)$ at a given time. This is consistent with the discussion in Sec. III that the OTOC tracks the lightcone of information dynamics for the infinite temperature state.

To obtain a more precise understanding, it is useful to think about the growth of the Heisenberg operator $W(t)$ in a complete basis of operators $\{\mathcal{S}\}$. The basis obeys the following normalization and completeness condition

$$\frac{1}{\text{tr}I} \text{tr}(\mathcal{S}^\dagger \mathcal{S}') = \delta_{\mathcal{S}\mathcal{S}'}, \quad \frac{1}{\text{tr}I} \sum_{\mathcal{S}} \mathcal{S}_{ab}^\dagger \mathcal{S}_{cd} = \delta_{ad} \delta_{bc}. \quad (75)$$

The conventional choice of the operator basis for qubit systems are the Pauli strings, which are products of Pauli operators or the identity operator on every site,

$$\mathcal{S} = \prod_{r=1}^N \sigma_r^{(s)}, \quad (76)$$

where $s = 0, 1, 2, 3$ stands for I , σ^x , σ^y and σ^z . Note that there are in total 4^N different Pauli strings for N qubits.

The Heisenberg operator $W(t)$ can be expanded in the basis

$$W(t) = \sum_{\mathcal{S}} \alpha(\mathcal{S}, t) \mathcal{S}. \quad (77)$$

Without loss of generality, we fix the the norm of $W(t)$ to be

$$\frac{1}{\text{tr}I} \text{tr}(W^\dagger W) = 1. \quad (78)$$

Since the time evolution is unitary, the normalization stay the same and $\sum_{\mathcal{S}} |\alpha(\mathcal{S}, t)|^2 = 1$ for all time. Hence, $|\alpha(\mathcal{S}, t)|^2$ can be interpreted as a probability distribution of the operator.

We also define a complete local operator basis at site r , denoted as \mathcal{S}_r . In qubit systems, the local basis includes three Pauli operators and the identity operator.

The generalization to qudit systems and fermion systems are discussed in the appendix Sec. B. In the general case, the local Hilbert space dimension is q , and there are q^2 local operators in the local operator basis.

Using the completeness relation, one can show that the average OTOC between $W(t)$ and all \mathcal{S}_r

$$\frac{1}{q^2} \sum_{\mathcal{S}_r} \frac{1}{\text{tr}I} \text{tr}(W^\dagger(t) \mathcal{S}_r^\dagger W(t) \mathcal{S}_r) = \sum_{\mathcal{S}_r=I} |\alpha(\mathcal{S}, t)|^2, \quad (79)$$

which measures the probability that $W(t)$ acts on site r as the identity operator, according to the probability distribution $|\alpha(\mathcal{S}, t)|^2$. Similarly, the average squared commutator is

$$\frac{1}{q^2} \sum_{\mathcal{S}_r} \frac{1}{\text{tr}I} \|[W(t), \mathcal{S}_r]\|_2^2 = 2 \sum_{\mathcal{S}_r \neq I} |\alpha(\mathcal{S}, t)|^2, \quad (80)$$

which is complementary to the average OTOC. Eq. (79) establishes a precise connection between OTOC and operator probability. In the summation in Eq. (79) and (80), the term with $\mathcal{S}_r = I$ does not have dynamics and can be separated from the other terms. Therefore we define the following average OTOC and squared commutator

$$\begin{aligned} \mathcal{F}(r, t) &= \frac{1}{q^2 - 1} \frac{1}{\text{tr}I} \sum_{\mathcal{S}_r \neq I_r} \text{tr}(W^\dagger(t) \mathcal{S}_r^\dagger W(t) \mathcal{S}_r) \\ &= \frac{q^2}{q^2 - 1} \sum_{\mathcal{S}_r \neq I} |\alpha(\mathcal{S}, t)|^2 - \frac{1}{q^2 - 1}, \\ \mathcal{C}(r, t) &= \frac{1}{q^2 - 1} \sum_{\mathcal{S}_r \neq I} \frac{1}{\text{tr}I} \|[W(t), \mathcal{S}_r]\|_2^2 = \\ &= \frac{2q^2}{q^2 - 1} \sum_{\mathcal{S}_r \neq I} |\alpha(\mathcal{S}, t)|^2. \end{aligned} \quad (81)$$

Starting with a simple local operator, the time evolution of the operator probability distribution can be very different between generic interacting systems and non-interacting systems. For instance, in non-interacting fermionic systems, a single-particle operator always remains single-particle. On the contrary, in interacting systems, a local operator tends to become as complex as possible in the late time. Maximal complexity for an initial traceless operator implies uniform distribution over the operator basis \mathcal{S} except for the identity. The identity operator is special since it is static under unitary time evolution. Therefore in systems with L qudits with local dimension q , we have

$$\lim_{t \rightarrow \infty} |\alpha(\mathcal{S}, t)| = \frac{1}{q^{2L} - 1} (1 - \delta_{\mathcal{S}, I}). \quad (82)$$

Based on Eq. (81), the late-time operator probability distribution determines the the late-time value of the average OTOC

$$\lim_{t \rightarrow \infty} \mathcal{F}(r, t) = -\frac{1}{q^{2L} - 1} \approx 0 \quad (83)$$

and

$$\lim_{t \rightarrow \infty} \mathcal{C}(r, t) = 2 \left(1 + \frac{1}{q^{2L} - 1} \right) \approx 2. \quad (84)$$

One can obtain the same late values of OTOC between $W(t)$ and a single local operator \mathcal{S}_r using Haar random unitary as the time evolution operator. These late-time values suggest that an operator becomes maximally complex and can be used to distinguish generic interacting many-body systems from non-interacting systems. We also note that the discussion above assumes no symmetry present. We will briefly discuss how symmetries impact scrambling dynamics in the Epilogue IX.

B. Scrambling dynamics in geometrically local systems

In Haar random unitary dynamics, there is no notion of space and time since $\mathcal{F}(r, t)$ reaches its final value in a single step for every r . In contrast, a physical many-body system only contains few-body interaction, such as spin-spin interactions or four-fermion interactions. A generic physical Hamiltonian of N sites is

$$H = \sum_b J_b(t) H_b \quad (85)$$

where H_b acts on a set of degrees of freedom labeled by b and J_b is the coupling strength which in general can be time-dependent. One can regard a quantum many-body systems as a hypergraph, one in which each site defines a vertex and each term in the Hamiltonian H_b defines a hyperedge e_b to be the set of vertices involved in H_b . This hypergraph completely determines the connectivity of the system. One can also generalize this description to unitary circuits, which are a tensor product of few-body unitaries,

$$U = \prod_b U_b. \quad (86)$$

From OTOC one can define a time scale t^* called scrambling time, at which $\mathcal{F}(r, t)$ relaxes to the final value ~ 0 for all sites r , given a Heisenberg operator $W(t)$ that is initially localized at one site. A natural question in this general setup is how the scrambling time t^* depends on the system size. The time scale is determined by both the connectivity of the hypergraph and the coupling strength J_b . While the complete answer to this question is not known, there exists extensive literature tackling specific regimes. We also note that although this general definition of a physical quantum many-body system seems obscure and unnecessarily complex from a conventional point of view, there currently exist experimental schemes allowing for tuning the connectivity between microscopic degrees of freedom [27], making quantum many-body systems with general graph structure a physically relevant topic.

To make our discussion tangible, let us restrict to cases where H_b only acts on two sites, describing a spin-spin interaction, for instance. In this case, the hypergraph reduces to a graph. One can imagine arranging the N qubits in a chain. The Hamiltonian can be written as

$$H = \sum J_{rr'}^{\alpha\beta}(t) \sigma_r^\alpha \sigma_{r'}^\beta \quad (87)$$

The strongest connectivity occurs when the graph is a complete graph where each qubit connects to every qubit with approximately the same interaction strength J . In such all-to-all connected models, it is typically found that the scrambling time scales logarithmically with N , $t^* \sim \log N$. Furthermore, in this case, given a qubit, all other qubits are equivalent. Therefore, $\mathcal{C}(r, t)$ does not have spatial dependence. Many calculations have shown that in the large N limit, $\mathcal{C}(r, t)$ in the early time takes an exponential growth form

$$\mathcal{C}(r, t) \sim \frac{1}{N} \exp(\lambda t), \quad (88)$$

where λ is called the Lyapunov exponent that is related to the coupling strength J . Here $\mathcal{C}(r, t)$ becomes $\mathcal{O}(1)$ when $t \sim \log N$, setting the scrambling time scale. It is suggested that this is the fastest scrambling time scale for physical systems with a proper normalization of $J_{rr'}$ [8, 28]. Significant research interest has been put into imposing bounds on the Lyapunov exponent to understand how fast quantum many-body system can process information. The chaos bound [11] concerns a finite temperature version of the OTOC and shows that $\lambda_L < 2\pi T$ in a quite general setting, leading to extensive studies on understanding and refining the bound and on operator growth in general, especially at finite temperature, e.g. [25, 26, 29–32]. We will briefly comment the notion of OTOCs at finite temperature and their connection to many-body quantum chaos in the Epilogue IX.

Moving away from all-to-all connected models, one should expect the scrambling time to increase as one reduces the connectivity since it will take longer for a local perturbation to spread over the system. One approach to reduce the connectivity is to require that $J_{rr'}$ decreases as a function of the distance $|r - r'|$ (Also see discussion about scrambling on sparse graphs [33–35]). As a result, $\mathcal{C}(r, t)$ generally develops a space-time profile, from which one can define an information lightcone by considering the contours of constant $\mathcal{C}(r, t)$,

$$\mathcal{C}(r, t_\theta(r)) = \theta \quad (89)$$

where θ is the threshold of the contour. The function $t_\theta(r)$ describes how fast information propagates, which depends on how fast the interaction decays over space. Substituting r with N , $t_\theta(N)$ also sets the scrambling time scale t^* . An interesting arises when $J_{rr'}$ decays algebraically as a function of $|r - r'|$, $J_{rr'} \sim 1/|r - r'|^\alpha$. One can show that as α increases and the interaction becomes more and more short ranged, $t^*(N)$ deviates from the fast scrambling behavior [36], and the asymptotic

form of $t_\theta(r)$ in scrambling systems undergoes a series of transitions, from logarithmic $t \sim \log^\eta(r)$ ($\eta > 1$) to algebraic $t \sim r^\xi$ ($\xi < 1$) and eventually when $\alpha > 1.5$ becomes linear $t \sim r$ [37, 38], indicating that information transport slows down from super-ballistic to ballistic. When $\alpha \rightarrow \infty$, the interaction becomes short-ranged and the usual Lieb-Robinson bound in Eq. (13) applies, restricting $t_\theta(r)$ to be at most ballistic [39–41].

Another line of research investigates how the presence of quenched disorder and localization affects the information lightcone [42–51]. Based on a phenomenological model called the weak link model [48], it was shown that starting from a model with short-ranged interaction, increasing the disorder strength impedes the information propagation and drives a series of transitions of the lightcone function from linear $t \sim r$ to algebraic $t \sim r^\xi$ ($\xi > 1$) and eventually becomes exponential $\log t \sim r$ when the system becomes many-body localized. Similar transitions are found in quasi-periodic systems as well [52, 53].

As this high level overview makes explicit, information scrambling in quantum many-body systems displays a rich set of behaviors dependent on both the connectivity and disorder. In the next section, we will focus on the case with short-ranged interaction where the information lightcone is linear and discuss the behavior of OTOCs in more detail. Furthermore, we will show explicitly that how OTOCs are calculated in several prototype models.

VI. SCRAMBLING DYNAMICS IN SYSTEMS WITH SHORT-RANGED INTERACTION

For a generic system with short-ranged interaction and no disorder, local operators spread ballistically, which has been shown in numerous systems including field theories [54, 55], free and integrable models [56, 57], interacting spin chains [58, 59] and circuit models [60–63]. In this case, we have $r(t) \sim v_B t$, where v_B is called the butterfly velocity. The typical behavior of a ballistically expanding $C(r, t)$ is sketched in Fig. 6. Fixing r and varying t , $C(r, t)$ grows from 0 to the saturation value, telling how the operator becomes complicated locally once the operator front reaches point r . On the other hand, fixing t and varying r , $C(r, t)$ decays from the saturation value to 0, as r exits the lightcone. These are the plots often used in the literature to characterize the behavior of $C(r, t)$.

In the local system, the Lieb-Robinson bound, already mentioned in Sec. II imposes substantial restrictions on the form of $C(r, t)$. Because of Lieb-Robinson,

$$C(r, t) \leq \| [W(t), \sigma_r] \|_\infty \leq c e^{\lambda_{LR}(t - r/v_{LR})} \quad (90)$$

From the Lieb-Robinson bound, it is natural to guess that

$$C(r, t) \sim \exp(\lambda(t - r/v_B)) \quad (91)$$

when C is far from saturation. This is indeed the correct form of many models in the large N s or semi-classically

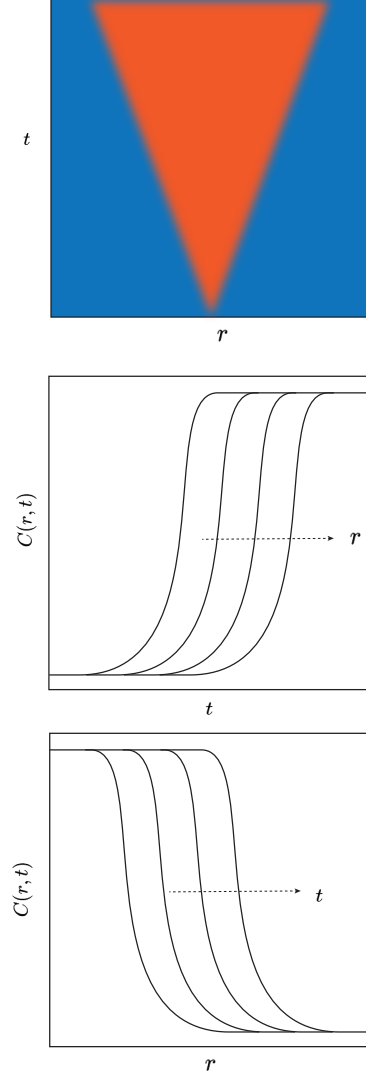


FIG. 6. Schematic sketch of $C(r, t)$ for local clean systems. In this case, the information lightcone is ballistic. The squared commutator $C(r, t)$ increases with t and decreases with r .

limit based on field theory calculations [54, 64]. However, in the random unitary circuit model [60, 61], the tail of the OTOC has a different behavior,

$$C(r, t) \sim \exp\left(-\frac{(x - v_B t)^2}{4D_B t}\right). \quad (92)$$

In contrast to large N and semi-classical calculation, this ballistically expanding wave has a diffusively broadened wavefront, meaning the scale over which C varies as a function of $u = r - t/v_B$ goes like $\sqrt{D_B t}$. Note that the random circuit model also has a version with a large number N_{dof} on each site, but while v_B and D_B depend on this number, but the holographic form is never obtained. Furthermore, the Lieb-Robinson bound also applies to the non-interacting system, where the squared commutator can be calculated exactly. In this case, we obtain

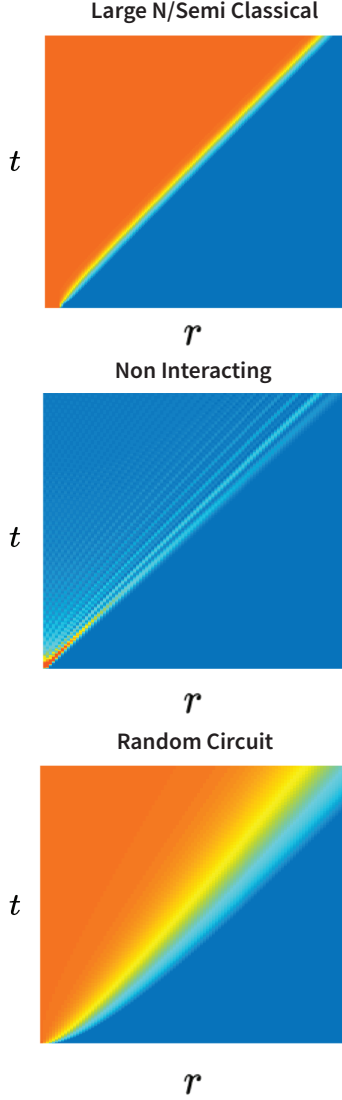


FIG. 7. Schematic illustration of the squared commutator $\mathcal{C}(r, t)$ with a ballistic propagating front in (a) large N /semi-classical systems, (b) non-interacting systems and (c) random unitary circuits.

another different behavior

$$\mathcal{C}(r, t) \sim \exp \left(\lambda \frac{(t - r/v_B)^{3/2}}{t^{1/2}} \right) \quad (93)$$

The typical behavior of the three classes of OTOC is illustrated in Fig. 7. One should not expect the non-interacting limit to be generic, but the spectre of multiple different universality classes allowed by Lieb-Robinson bound is certainly raised. There seem many possibilities.

To understand the generic behavior of OTOC, let us look at the constraint on the functional form of OTOC imposed by the Lieb-Robinson bound. The Lieb-Robinson bound implies that

- (i) $\mathcal{C}(r, t)$ decays exponentially or faster with r , fixing

t .

- (ii) $\mathcal{C}(r, t)$ grows exponentially or slower with t , fixing r .

- (iii) $\mathcal{C}(vt, t)$ decays exponentially or faster with t for $v > v_{LR}$.

These constraints are most restrictive in the earlier growth regime where $\mathcal{C}(r, t)$ is still small. A general form [59, 65] that satisfies these constraints is

$$\mathcal{C}(r, t) = \exp \left(\frac{\lambda(t - r/v_B)^{1+p}}{t^p} \right). \quad (94)$$

This growth form unifies the three classes mentioned above into a single framework by including one additional parameter p , called the broadening exponent. The large N and semi-classical result fits the form with $p = 0$ (no broadening). The random circuit result fits the form with $p = 1$ in $d = 1$ (diffusive broadening). The non-interacting fermion result fits with $p = 1/2$ in $d = 1$.

The physics of the general growth form and the broadening exponent p are as follows. Given the general shape in Eq. (94), the contours $\mathcal{C}(r, t) = \theta$ obey

$$r_\theta = v_B t + \left(\frac{t^p}{\lambda} \log \frac{1}{\theta} \right)^{\frac{1}{1+p}}. \quad (95)$$

Hence, no matter the value of θ , asymptotically one has

$$\lim_{t \rightarrow \infty} \frac{r_\theta}{t} = v_B. \quad (96)$$

However, at any finite t , the contour has an extra sub-ballistic time dependence going like $t^{\frac{p}{1+p}}$ which is due to the wavefront broadening. As a result, the spatial distance between two contours at a give t is

$$\delta r = r_{\theta_1} - r_{\theta_2} \sim t^{\frac{p}{1+p}}. \quad (97)$$

This is the key difference between the large N /semi-classical models and the other models such as non-interacting systems and random circuit models. In the large N /semi-classical models, δr does not grow with t as $t \rightarrow \infty$. Although the non-interacting system is not scrambling and should not be expected to be generic, the difference between the large N /semi-classical models and random circuit models, both strongly interacting and scrambling, requires understanding.

A. Prototype models

Before understanding the mechanism of the various growth behavior of OTOC and the different broadening exponent p , let us first sketch how OTOC is calculated in various models and how the wavefront broadening occurs microscopically.

1. Free fermions

We start with non-interacting systems. Although one should not expect these models to be generic, they provide important lessons on possible functional forms regarding the tail of the OTOC since the Lieb-Robinson bound applies to the non-interacting systems as well. Consider a non-interacting majorana system described by the Hamiltonian

$$H = \frac{1}{2} \sum_{a,b} h_{rr'} \chi_r \chi_{r'} \quad (98)$$

where χ is the majorana operator that obeys the commutation relation $\{\chi_r, \chi_{r'}\} = \delta_{rr'}$. The Hermiticity of H requires that $h_{rr'} = -h_{rr'}^*$ and $h_{rr'} = -h_{r'r}$. Therefore h is a purely imaginary antisymmetric matrix. In addition, we assume that H is translational symmetric and thus can be diagonalized by Fourier transformation. Introduce $\chi_k = \sum_r \frac{1}{\sqrt{N}} e^{ikr} \chi_r$ satisfying $\{\chi_k, \chi_{k'}\} = \delta_{k,-k'}$. Then the Hamiltonian can be written as

$$H = \frac{1}{2} \sum_k \epsilon_k \chi_{-k} \chi_k. \quad (99)$$

The spectrum ϵ_k is an odd function in k because matrix h is imaginary and antisymmetric. The goal here is to calculate the OTOC

$$F(r, t) = \frac{1}{\text{tr} I} \text{tr}(\chi_0(t) \chi_r \chi_0(t) \chi_r) \quad (100)$$

or equivalently the squared anticommutator defined in the appendix

$$C(r, t) = \frac{4}{\text{tr} I} \text{tr}(\{\chi_0(t), \chi_r\} \{\chi_0(t), \chi_r\}). \quad (101)$$

Using the Hamiltonian in the momentum space, one can show that the Heisenberg operator $\chi_0(t)$ is

$$\chi_0(t) = \sum_r g(r) \chi_r \quad (102)$$

where

$$g(r) = \sum_k \frac{1}{N} e^{i\epsilon_k t - ikr} = \frac{1}{2\pi} \int e^{i\epsilon_k t - ikr} dk \quad (103)$$

Because $\epsilon_k = -\epsilon_{-k}$, the coefficient $g(r, t)$ is real as expected from expanding the Hermitian operator $\chi_0(t)$. The fact that only a single majorana operator appears in the expansion is because of the non-interacting Hamiltonian. In general, majorana strings of all lengths would appear. From $g(r)$, one can obtain the OTOC as

$$C(r, t) = 4g^2(r, t) \quad (104)$$

Therefore, the behavior of $C(r, t)$ is controlled by $g(r, t)$, which can be analyzed using saddle point approximation. We expand the function around k_0 as

$$g(r, t) \sim \int \frac{d\delta k}{2\pi} e^{i(v(k_0)t - x)\delta k + \frac{i}{2}\epsilon_{k_0}^{(2)} t \delta k^2 + \frac{i}{6}\epsilon_{k_0}^{(3)} t \delta k^3 + \dots}, \quad (105)$$

where $v(k_0)$ is the group velocity at k_0 . One can always find suitable k_0 making the first derivative term vanish for $|x| < \max(|v(k_0)|)t$, while it is not possible to do so if $|x| > \max(|v(k_0)|)t$. This leads to change of behavior of $g(x, t)$ at $|x| = \max(|v(k_0)|)t$, indicating that the butterfly velocity v_B is the maximal velocity. In the region $x > v_B t$, the first order derivative term is always nonzero. We keep up to the third order term and obtain that

$$\begin{aligned} g(r, t) &\sim \frac{1}{2\pi} \int d\delta k e^{i(v_B t - r)\delta k + \frac{i}{6}\epsilon_{k_0}^{(3)} t \delta k^3} \\ &\sim \frac{1}{t^{1/3}} \text{Ai}\left(\frac{r - v_B t}{(-\epsilon_{k_0}^{(3)} t/2)^{1/3}}\right) \end{aligned} \quad (106)$$

where $\text{Ai}(Z)$ is the Airy function. Note that here $\epsilon_{k_0}^{(3)}$ is negative since the group velocity is maximal at k_0 . In the limit that $r - v_B t \gg |\partial_k^3 \epsilon(k_0) t/2|^{1/3}$, we can use the asymptotic form of the Airy function and obtain Eq. (93). In this case, the wavefront broads subdiffusively with $\delta r \sim t^{1/3}$ and the broadening exponent $p = 1/2$. On the other hand, in the long time limit $t \gg r/v_B$, one can find k_0 that makes the first derivative vanish and perform the Gaussian integral to get $g(r, t) \sim 1/t^{1/2}$. As a result, in the long time limit $C(r, t)$ decays to 0 as $1/t$ in the non-interacting systems. This is in sharp contrast with chaotic system where $C(r, t)$ approaches 2 in the long time limit. These results from saddle point analysis can be explicitly checked by exact calculation using nearest neighboring hopping model given by $h_{rr'} = i\delta_{r,r'+1} - i\delta_{r,r'-1}$. In this case, $\epsilon_k = \sin k$ and $g(r, t) = J_r(t)$, a Bessel function.

2. coupled Sachdev-Ye-Kitaev model

The large N /semi-classical setting is another class of typically interacting models for which scrambling dynamics and OTOC are tractable. A representative model in this class is the Sachdev-Ye-Kitaev model [66, 67] (also see a recent review [68]) describing a cluster of N interacting Majorana fermions,

$$H = \sum_{i_1 < i_2 < i_3 < i_4} j_{i_1 i_2 i_3 i_4} \chi_{i_1} \chi_{i_2} \chi_{i_3} \chi_{i_4}, \quad (107)$$

where χ_i is Majorana operator obeying the usual commutator $\{\chi_i, \chi_j\} = \delta_{ij}$. The coupling constants $j_{i_1 i_2 i_3 i_4}$ are uncorrelated Gaussian variable with zero mean and standard deviation $\langle j^2 \rangle = 6J^2/N^3$, where the factors of N is required to make sure the energy of the system is extensive, i.e., scaling linearly with N .

One can generalize the SYK model to higher dimensions by considering M clusters of N fermions [64, 69–71]. Each cluster only interacts with its nearest neighbors. The Hamiltonian contains both on-site terms and bond terms,

$$H = \sum_r H_r + \sum_{\langle rr' \rangle} H_{rr'} \quad (108)$$

where H_r is the usual SYK Hamiltonian in Eq. (107) and the bond term is given by

$$H_{rr'} = \sum_{\substack{1 \leq j < k \leq N \\ 1 \leq l < m \leq N}} J'_{jklm, rr'} \chi_{j,r} \chi_{k,r} \chi_{l,r'} \chi_{m,r'}. \quad (109)$$

The OTOC of the generalized SYK model can be calculated using the same diagrammatic approach in the large N limit. The details of the calculation can be found in [64, 72], showing that the OTOC takes the simple exponential form in Eq. (91) up to higher order corrections.

3. Random circuit model

Next, consider the case of a spin chain where the time evolution is taken to consist of alternating even and odd layers of random two-qubit gates. The tensor structure gives the unitary operator that governs the dynamics in Fig. 2 where each block is independent Haar random unitary with dimension 4×4 for qubits or $q^2 \times q^2$ in general for local dimension q . This model is called a random unitary circuit, a tractable many-body model for studying entanglement generation [73] and operator dynamics [60, 61]. There are also generalizations of the random unitary circuit to respect charge conservation [74, 75], dipolar conservation [76] or other kinetic constraints, which are important for studying the interplay between transport phenomena and scrambling. In these random circuit models, the random average of the local unitary operator usually map the quantum many-body models to statistical models that are easier to handle while retain the universal aspects of the quantum many-body dynamics.

Let us focus on the random circuit model without any structure except for the brickwork structure. The idea to calculate the OTOC is to track the Haar averaged time evolution of the operator probability distribution,

$$|\alpha(\mathcal{S})|^2 = \frac{1}{q^{2N}} |\text{tr}(\mathcal{S}^\dagger W)|^2 \quad (110)$$

where \mathcal{S} is an operator string defined in appendix B 1.

In the random unitary circuit, each Haar random unitary can be averaged out independently. Consider applying a single local unitary gate U to site r and $r+1$ to the Heisenberg operator. The updated operator probability is given by

$$|\alpha(\mathcal{S})|^2 = \frac{1}{q^{2N}} \mathbb{E} |\text{tr}(\mathcal{S} U^\dagger W U)|^2 \quad (111)$$

It is instructional to consider only two sites first. It is straightforward to show that the Haar average leads to

$$\begin{aligned} & |\alpha'(\mathcal{S})|^2 \\ &= \sum_{\mathcal{S}'} \left[\delta_{I,\mathcal{S}} \delta_{I,\mathcal{S}'} + \frac{1}{q^4 - 1} (1 - \delta_{I,\mathcal{S}})(1 - \delta_{I,\mathcal{S}'}) \right] |\alpha(\mathcal{S}')|^2 \end{aligned} \quad (112)$$

Notice the remarkable feature that the updated operator probability only depends on the operator probability before the update but not the amplitude. This is a simplification due to the Haar random, but not true in general many-body systems. In addition, the identity operator stays the identity operator as expected from the unitary time evolution. The non-identity operators become uniformly distributed non-identity operators because of the scrambling nature of the Haar random unitary. To proceed, each operator string is mapped to a binary string. On each site, the identity operator is mapped to 0 and the others are mapped to 1. The probability of the binary string $P(\mathcal{S})$ is the sum of the probability of operators mapping to the same string. Then the transition rule is given by

$$\begin{aligned} P(00, t+1) &= P(00, t) \\ P(01, t+1) &= \frac{1}{q^2 + 1} (P(11, t) + P(10, t) + P(01, t)) \\ P(10, t+1) &= \frac{1}{q^2 + 1} (P(11, t) + P(10, t) + P(01, t)) \\ P(11, t+1) &= \frac{q^2 - 1}{q^2 + 1} (P(11, t) + P(10, t) + P(01, t)) \end{aligned} \quad (113)$$

Since in Haar random circuit, each unitary is independent, the transition rule above also hold locally when a local unitary u acts on on site r and $r+1$. In this case, the binary string probabilities only change locally on site r and $r+1$ according to the transition rule given above. It is useful to consider the probability that the last 1 in the binary string ends at r , $P_{\text{end}}(r)$. Based on Eq. (113), applying the local unitary u_{rr+1} updates P_{end} as follows

$$\begin{aligned} P'_{\text{end}}(r) &= \frac{1}{q^2 + 1} (P_{\text{end}}(r, t) + P_{\text{end}}(r+1, t)) \\ P'_{\text{end}}(r+1) &= \frac{q^2}{q^2 + 1} (P_{\text{end}}(r, t) + P_{\text{end}}(r+1, t)) \end{aligned} \quad (114)$$

Notice that $(P_{\text{end}}(r, t) + P_{\text{end}}(r+1, t))$ is conserved as expected. The unitary $u_{r,r+1}$ just re-distributes them so that the operator has higher probability to end at $r+1$, leading to expansion. Recall that the unitary circuit acts on the even and odd bond alternatively. The layer of even (odd) t acts on even (odd) bond. To take account the combined effect of even and odd layer of the unitary circuit, it is more convenient to track the sum of P_{end} on even bonds, denoted $P_{\text{end}}(b)$, after each even layer. Because of Eq. (114), $P_{\text{end}}(b)$ for even b fully specifies $P_{\text{end}}(r)$ after the even unitary layer. One can show that P_{end} obeys

$$\begin{aligned} P_{\text{end}}(b, t+2) &= \left(\frac{q^2}{q^2 + 1} \right)^2 P_{\text{end}}(b+2, t) \\ &+ \left(\frac{1}{q^2 + 1} \right)^2 P_{\text{end}}(b-2, t) \\ &+ \frac{2q^2}{(q^2 + 1)^2} P_{\text{end}}(b, t) \end{aligned} \quad (115)$$

This equation describes a biased random walk. In the continuum limit, the equation becomes a biased diffusion equation

$$\partial_t P_{\text{end}}(r, t) = v_B \partial_r P_{\text{end}}(r, t) + D \partial_r^2 P_{\text{end}}(r, t) \quad (116)$$

where

$$v_B = \frac{q^2 - 1}{q^2 + 1}, \quad D = \frac{2q^2}{(q^2 + 1)^2} \quad (117)$$

The solution of the biased diffusion equation with initial condition $\delta(r)$ is

$$P_{\text{end}}(r, t) = \frac{1}{\sqrt{4\pi Dt}} \exp\left(-\frac{(r - v_B t)^2}{4Dt}\right) \quad (118)$$

To obtain the squared commutator, it is reasonably to assume that operator on every site behind the end point of the operator is in local equilibrium. As a result, from Eq. (81)

$$\begin{aligned} \mathcal{C}(r, t) &= \frac{2q^2}{q^2 - 1} \sum_{\mathcal{S}, r \neq I} |\alpha(\mathcal{S})|^2 \sim 2 \int_r^\infty P_{\text{end}}(r', t) dr' \\ &= 1 + \text{erf}\left(-\frac{(r - v_B t)}{\sqrt{4Dt}}\right). \end{aligned} \quad (119)$$

It exhibits ballistic expansion and diffusive broadening of the wavefront. When $t > r/v_B$, it quickly saturates to the final 2, indicating scrambling. The tail behavior of $\mathcal{C}(r, t)$ can be obtained expanding the error function in the limit that $r - v_B t \gg \sqrt{Dt}$. This leads to the growth form given in Eq. (92), which is in contrast with the growth form obtained in the semi-classical/large N and ADS/CFT models. Physically, the Gaussian tail of the squared commutator obtained in the random circuit model relies on two factors. First, the endpoint of the operator undergoes a random walk biased towards expansion. Second, the operators behind the endpoint immediately reach the local equilibrium because of the Haar random unitary.

4. Brownian models

We have seen that the random circuit model and the SYK model give rise to distinct functional forms of the OTOC. Both cases feature a ballistic lightcone, but the wavefront broadens diffusively in the random circuit model while the wavefront is sharp in the SYK model. The question then arises which, if any, of these characteristic shapes describes the generic case with a finite local Hilbert space dimension. Unfortunately, this question cannot be reliably answered using small sized numerical simulations. These exhibit ballistic expansion with some broadened wavefront, but it is unclear if the broadening will vanish in a large system, tend to the diffusive limit, or have some other characteristic form. Non-interacting

particles exhibit ballistic expansion of \mathcal{C} with yet another characteristic broadening of the wavefront (\mathcal{C} does not saturate at late time in this model, instead falling back to zero). One should not expect the non-interacting limit to be generic, but the spectre of multiple different universality classes is certainly raised.

To answer this question, we now introduce another class of models known as the Brownian models [10, 28, 77–81], in which the interaction between the underlying degrees of freedom are stochastic variables. Here we consider a specific version of the model with spin-spin interactions, called the Brownian coupled cluster model. Like the random circuit model, it features a random time-dependent Hamiltonian, but unlike the random circuit model, it has a large N limit. Using it, we will develop a physical picture of why $p = 1$ is generic for one-dimensional chaotic systems. The model can be defined in any dimension, but here we continue to focus on $d = 1$. The degrees of freedom are arranged in clusters which are then connected into a one-dimensional array. Every cluster contains N spin-1/2 degrees of freedom, and there are L clusters. The Hamiltonian is time-dependent and consists of two kinds of terms, within-cluster interactions and between-cluster interactions. In order to avoid mathematical complexities associated with stochastic calculus, it is simplest to present the model in discrete time.

The time evolution operator is

$$U(t) = \prod_{m=1}^{t/dt} \exp\left(-i \sum_r H_r^{(m)} - i \sum_{\langle rr' \rangle} H_{rr'}^{(m)}\right), \quad (120)$$

with m a discrete time index. The within-cluster terms and the between-cluster terms are

$$H_r^{(m)} = J_{m,r,a,b}^{\alpha\beta} \sigma_{r,a}^\alpha \sigma_{r,b}^\beta \quad (121)$$

$$H_{rr'}^{(m)} = g \tilde{J}_{m,r,r',a,b}^{\alpha\beta} \sigma_{r,a}^\alpha \sigma_{r',b}^\beta \quad (122)$$

where $\alpha, \beta \in \{0, 1, 2, 3\}$, $a, b = 1, \dots, N$ label spins within a cluster, r, r' label clusters (sometimes called sites), and $\langle rr' \rangle$ means nearest neighbors. At each time step, the models contains two sets of uncorrelated random variables J and \tilde{J} with mean zero and variance $\frac{1}{8(N-1)}dt$ and $\frac{1}{16N}dt$, respectively.

In the limit that $dt \rightarrow 0$, one can formulate a stochastic differential equation for the time evolution operator. From it, one can derive a master equation for the operator probabilities $|\overline{c(\mathcal{S})}|^2$ averaged over circuit realizations, i.e., over realizations of the couplings J and \tilde{J} . We will not get into the details of these equations here, but see Ref. [78] for complete details. The only important property we need is that $|\overline{c(\mathcal{S})}|^2$ depends only on the total number of non-identity Pauli operators on each cluster. This is technically an approximation, but it holds after a short time even if the initial condition does not obey it because the circuit average erases any distinction between the different Pauli operators. The total number of non-identity Pauli operators in P_S on cluster r is called the weight of the cluster and is denoted $w_r(\mathcal{S})$.

In this model, the operator averaged squared commutator \mathcal{C} has a cluster index as well as the index of the qubit within a cluster,

$$\mathcal{C}^a(r, t) = \frac{1}{3\text{tr}I} \sum_{\mathcal{S}_{r,a}} \|W(t), \mathcal{S}_{r,a}\|_2^2 \quad (123)$$

According to Eq. (81), $\mathcal{C}^a(r, t) = \frac{8}{3} \sum_{\mathcal{S}_{r,a} \neq I} |\alpha(\mathcal{S}, t)|^2$. It is convenient to analyze the $\mathcal{C}^a(r, t)$ averaged over all spins within a cluster r

$$\phi(r, t) \equiv \frac{1}{N} \sum_a \mathcal{C}^a(r, t) = \frac{8}{3} \sum_{\mathcal{S}} w_r(\mathcal{S}) |\alpha(\mathcal{S})|^2 \quad (124)$$

which measures the averaged number of non-identity operator appears over the N spins, or the averaged operator weight $\langle w_r \rangle$ within the cluster r . At early time, $\phi(r, t) \approx 0$ while at late time it saturates to $\phi(r, t) = 2$ as the usual case.

Like the Haar random circuit, using random averaging of coupling, one can derive a master equation governing the dynamics of the operator probability $|\alpha(\mathcal{S})|^2$. When N is small, it can be shown that $\mathcal{C}(r, t)$ obeys a drift-diffusion equation as in the random circuit model. This leads to a circuit averaged $\phi(r, t)$ obeying the universal form Eq. (94) with $p = 1$. Hence the Brownian coupled cluster model recovers the result of the random circuit model at small N .

At infinite N , something very different occurs. It can be shown that $\phi(r, t)$ obeys a so-called Fisher-Kolmogorov-Petrovsky-Piskunov (FKPP) type equation of the form

$$\partial_t \phi = \frac{3}{2} (2 - \phi) \left(\frac{g^2}{2} \partial_r^2 \phi + (1 + g^2) \phi \right). \quad (125)$$

Here g is the ratio of the strength of the between-cluster and within-cluster terms, and we have taken a continuum limit, which is qualitatively accurate. Although we will not explain its detailed derivation, one can see that this equation contains three essential pieces of physics: exponential growth in time, spreading in space, and saturation. The FKPP equation is very well known and describes a wide variety of physical processes including the propagation of combustion waves, the dynamics of invasive species, and the physics of certain quantum chromodynamics processes.

The key physical property of the FKPP equation is that, starting from a localized source, it supports travelling wave solutions with $\mathcal{C}(r, t) = f(r - v_B t)$ where $v_B = \sqrt{18g^2(1 + g^2)}$ is the butterfly velocity. Well ahead of the front at $r = v_B t$, the waveform is

$$\phi(r, t) \sim e^{\lambda_L(t - r/v_B)}, \quad (126)$$

which is Eq. (94) with $p = 0$. Hence the Brownian coupled cluster model also recovers the physics of large N and semi-classical result. The exponent $\lambda_L = 6(1 + g^2)$ is an example of a quantum Lyapunov exponent.

Given the large and small N limits, the next question is how they are connected as N is varied. Physically, the infinite N limit functions to suppress quantum fluctuations, so that one may view the distribution $|\overline{c(\mathcal{S})}|^2$ as being concentrated on a single weight configuration. At finite N , quantum fluctuations occur, meaning that the distribution $|\overline{c(\mathcal{S})}|^2$ now assigns non-vanishing probability to different operators weight configurations. It is important to understand that these fluctuations are proper quantum fluctuations. They are a consequence of the fact that $W(t)$ is a superposition of many different Pauli strings of different weights. In particular, the randomness associated with the couplings J and \tilde{J} has already been averaged over and no longer enters the description. In essence, the circuit average serves to dephase the quantum operator amplitudes and convert the Heisenberg equation of motion for the operator amplitudes into a master equation for the operator probabilities.

Following Ref. [78], we will call these quantum fluctuations ‘noise’. In an abuse of notation where $\phi(r, t)$ now represents a noisy field, we obtain a noisy FKPP equation,

$$\begin{aligned} \partial_t \phi &= 3(1 - \phi)f(\phi) + \sqrt{\frac{1}{N}}(2 - \phi/2)f(\phi)\eta(r, t), \\ f(\phi) &= \left(\frac{g^2}{2} \partial_r^2 + (1 + g^2) \right) \phi \end{aligned} \quad (127)$$

where $\eta(r, t)$ is a white noise term representing quantum fluctuations. This noise term, while suppressed by $1/N$, has a dramatic effect on the physics. Notice also that it multiplicative noise, vanishing when $\phi = 0$, so it respects the causal structure.

The main effect of the noise term is to make the front position noise dependent. This means that the front continues to move with velocity v_B , but it is also randomly buffeted forward and backward as in a random walk. Within a particular noise realization, the wavefront is sharp and exhibits $p = 0$. However, the physical quantity in the quantum problem is the noise averaged value of ϕ . Close enough to the physical front at $r = v_B t$, the random walk nature of front position inevitably manifests and smears the sharp $p = 0$ front into a diffusive $p = 1$ front. Using the noisy FKPP literature [82], Ref. [78] showed that the corresponding diffusion constant was $D \sim 1/\log^3 N$ at large N , a remarkably large value relative to standard $1/N$ corrections.

B. Phenomenological description

Given these developments, a conjecture and a corresponding physical picture naturally present themselves. We claim that, due to the inevitable presence of quantum fluctuations, generic one-dimensional quantum chaotic systems always have squared commutators obeying the universal form in Eq. (94) with $p = 1$. There is an analogous claim in higher dimensions, where the value of p

depends on the dimension and is related to a random surface growth problem (the Kardar-Parisi-Zhang universality class). Based on discussions in previous sections, the key pieces of evidence in favor of this claim are the random circuit model and the Brownian coupled cluster model. Interestingly, FKPP-like equations have also been obtained in various large N and weak coupling calculations of squared commutators. These were all noiseless equations, but surely once quantum fluctuations are included, the dynamics will be governed by an FKPP-like equation with multiplicative noise and a corresponding broadened front.

Based on the previous discussion on the random circuit, SYK model, and Brownian coupled cluster, the universal features of the dynamics of OTOC is

1. ballistic expanding
2. late time saturation
3. local exponential (Lyapunov) growth
4. random walk near the wavefront

A phenomenological description that captures all the key features is following:

$$\mathcal{C}(r, t) \sim \frac{1}{\sqrt{2\pi Dt}} \int d\Delta r \frac{e^{-\Delta r^2/2Dt}}{e^{\lambda((r+\Delta r)/v-t)} + 1} \quad (128)$$

which is a convolution between a Fermi-Dirac function and a Gaussian distribution, describing a travelling wave moving at velocity v . In the limit that $\lambda \rightarrow \infty$, the Fermi-Dirac distribution function becomes a step function, and Eq. (128) recovers the behavior of the random circuit model. On the other hand, in the limit that $D \rightarrow 0$, the Gaussian distribution becomes a delta function, and Eq. (128) reduces to the exponential form for the large N models. Let us work with the dimensionless variables

$$\tilde{r} = \frac{rv}{D}, \quad \tilde{t} = \frac{tv^2}{D}, \quad \xi = \frac{\lambda D}{v^2}. \quad (129)$$

The phenomenological description becomes

$$\mathcal{C}(r, t) = \frac{2}{\sqrt{2\pi}} \int d\Delta r \frac{e^{-\Delta r^2/2}}{e^{\xi\sqrt{\tilde{t}}(\Delta r + (r-t)/\sqrt{\tilde{t}})} + 1} \quad (130)$$

whose behavior is controlled by a single parameter ξ . For simplicity, we have dropped the tilde in \tilde{r} and \tilde{t} . The integration does not have a closed form, but we understand its behavior in different space-time regimes.

First, one can show that $\mathcal{C}(r, t) = 1$ when $r = t$, setting the wavefront as expected. When $(r - t)/\sqrt{t} \leq \text{const.}$, the Fermi-Dirac function approaches to a step function in the large t limit, and

$$\mathcal{C}(r, t) \approx \text{erfc}\left(\frac{r - t}{\sqrt{2t}}\right). \quad (131)$$

On the other hand, when $r - t > \xi t$, the exponential term dominates the denominator and the integration leads to

$$\mathcal{C}(r, t) \approx 2 \exp(\xi((1 + \xi/2)t - r)), \quad (132)$$

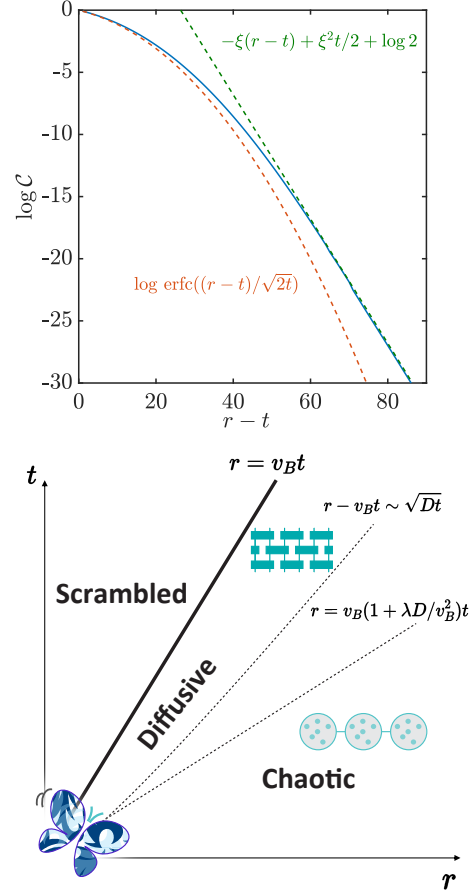


FIG. 8. A schematic illustration of the behavior of the squared commutator $\mathcal{C}(r, t)$ in different space-time region.

which recovers the large N form. Interestingly, both the Lyapunov exponent and the butterfly velocity increase by a factor $(1 + \xi/2)$. We perform the integration numerically and plot $\log \mathcal{C}$ as a function of $r - t$ fixing t in Fig. 8(a) which clearly demonstrates that $\log \mathcal{C}$ interpolates between the two limiting cases, the error function and the exponential function.

Based on the discussion above, one arrives at the following picture of scrambling dynamics in an extended quantum many-body system with short-ranged interaction and finite local Hilbert space dimension. The information propagates ballistically with a butterfly speed v_B . Due to inevitable quantum fluctuation, in the space-time regime near $r - v_B t \sim \sqrt{Dt}$, which we denote as diffusive regime, $\mathcal{C}(r, t)$ is characterized by a diffusive broadened wavefront. In this regime, there is no well-defined Lyapunov exponent that is independent of position and velocity. However, far ahead of the wavefront $r - v_B t > \lambda D/v_B t$, $\mathcal{C}(r, t)$ grows exponentially with a well-defined Lyapunov exponent, and thus we denote this regime as the chaotic regime.

Still, it would be nice to check this claim that the wavefront broads diffusely in a quantum spin chain with no

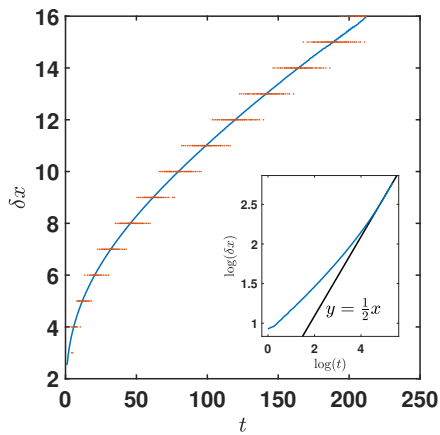


FIG. 9. Separation between two different contours of constant C as a function of time for the mixed-field Ising model. The inset shows a log-log plot of the same data. The asymptotic approach to a slope of $1/2$, corresponding to $p = 1$, is clearly visible in the data. Taken from Fig. 4(b) of [78].

randomness in space or time and generic chaotic interactions. More generally, the preceding discussion did not provide a method to calculate squared commutators for generic physical systems. One may wonder if there exists general methods or numerical algorithm to study OTOC for these systems. This will be the topic of the next section. Before going to the details of these methods, we would like to point out that numerical results strongly support diffusive broadening of the information wavefront in spin chains with large system sizes. Fig. 9 shows data obtained from this MPO approach for the mixed field Ising model at infinite temperature. The simulation is performed for $n = 201$ spins out to quite a long time, several hundred $1/J$. It has been checked that the results are converged in bond dimension with a bond dimension as low $\chi = 32$. What is plotted are the contours of the constant squared commutator. The inset shows the difference between different contours as a function of time on a log-log plot. Eq. (95) predicts that the difference between contours should go like $t^{\frac{p}{p+1}}$, so on a log-log plot the data should approach a straight line of slope $\frac{p}{p+1}$. This is precisely what occurs with an asymptotic slope of $1/2$ corresponding to $p = 1$. Hence we verify that for a large, non-random chaotic spin chain, the operator growth dynamics is ballistic with a diffusively broadened front exactly as predicted.

The chaotic regime ahead of the front should also be present but is difficult to observe. Based on the picture shown in Fig. 9(b), the size of the chaotic regime is determined by the ratio $v_B^2/\lambda D$. Therefore, one may observe the exponential growth in systems with large v_B but small λ , as shown in [83].

VII. NUMERICAL METHODS

In this section, we discuss some existing numerical methods to calculate the OTOC in many-body systems, including commenting on their applicability and limitations. The numerical methods can be roughly divided into two categories, exact diagonalization and tensor-networks. There are many other wholly or partially numerical approaches to calculating OTOCs, but these are among the most general purpose.

A. Exact diagonalization and Krylov space method

We first discuss the exact diagonalization based method to compute the OTOC in the system described by Hamiltonian H . In this case, it is more convenient to consider the OTOC in the form of $F = \text{tr}(W(t)\sigma W(t)\sigma)$, where $W(t)$ is the time evolved Heisenberg operator and σ is a local probe operator. The most straightforward method to compute OTOC is to perform a full exact diagonalization on H to obtain the eigenvector $|n\rangle$ as well as the eigenvalues ϵ_n . Then the OTOC can be evaluated as

$$F(t) = \frac{1}{2^N} \sum_{m,n,p,q} e^{i\epsilon_{nm}t} W_{nm} \sigma_{ml} e^{i\epsilon_{pq}t} W_{pq} \sigma_{qn} \quad (133)$$

where $\epsilon_{mn} = \epsilon_m - \epsilon_n$. The matrix W and σ is the in the eigenstate basis, which only need to compute once to calculate OTOC at different time. Although this is the simplest and numerical exact method, it suffers severely from small system size. The bottleneck is the full diagonalization of H and storing the eigenstates, which can be done for up to 15 qubits – It takes about 40G memory to just store the whole set of eigenstates.

One can avoid exact diagonalization by implementing the Heisenberg time evolution using Krylov method. The Krylov basis can be generated by applying Hamiltonian to the operator iteratively k times, where $k+1$ sets the effective Hilbert space dimension. Specifically, we have,

$$W^{(n)} = HW^{(n-1)} - W^{(n-1)}H, \quad 1 \leq n \leq k \quad (134)$$

The Krylov method is also numerically exact. It does not require diagonalizing the Hamiltonian, but it requires regenerating the basis by applying the Hamiltonian to the operator multiple times at each step, which can be time consuming. This method is limited by storing the large matrix of $W(t)$. Initially, W is a local operator in the form of a sparse matrix. The complexity of $W(t)$ increases with time, and in the late time, $W(t)$ becomes dense and requires a huge memory to store. As a result, this operator-Krylov method, similar to the naive exact diagonalization method, can also only work for up to 15 spins.

The difficulty of storing the full Heisenberg operator can be circumvented by calculating the OTOC in the Schrodinger equation and using the typicality of random

representation of an MPO is similar to MPS as shown below,

$$W = \begin{array}{c} \text{---} \square \text{---} \square \text{---} \square \text{---} \square \text{---} \dots \text{---} \square \text{---} \square \text{---} \square \text{---} \square \text{---} \end{array} \quad (139)$$

The MPS requires to store $2L$ matrices, the 2 coming from the physical index \uparrow and \downarrow , in total $2L\chi^2$ complex numbers. Therefore MPS is a very compact approach to represent a wavefunction that contains 2^L numbers. As expected, an MPS of a given bond dimension χ can only represent a tiny portion of the Hilbert space, characterized by low entanglement entropy. The entanglement entropy of an MPS with bond dimension χ is maximally $\log \chi$, a constant, while the entanglement entropy of a random state in the Hilbert space scales linearly with L . Fortunately, the entanglement entropy of the ground state of one dimensional gapped systems exhibits area law, i.e., does not scale with system size, and thus can be captured accurately.

A large toolbox for manipulating MPS/MPO has been developed over the years [89, 90]. The key idea behind studying dynamics using MPS/MPO is to evolve the state and operator while preserving the matrix product form. However, unlike searching for the ground state, the complexity of the simple initial states and initial operators increases over time, and in late time, the states exhibit volume law entanglement entropy. As a result, at some point during the evolution, usually a short time scaling as one over the interaction strength, the state cannot be captured faithfully by an MPS with a reasonable bond dimension. In practice, the quantities of physics interests are local observable and correlation functions, instead of the entire quantum state. To obtain the physical observable $\langle O(t) \rangle$ at a given time, one can repeat the simulation with increasing bond dimension, and the result can be trusted if it converges with the bond dimension.

There are two major approaches to evolve MPS/MPO: time evolving block decimation (TEBD) and time dependent variational principle (TDVP). In TEBD, the local unitary gate is directly applied to the MPS and increases the bond dimension of MPS. Then the MPS is truncated so that the bond dimension stays the same, leading to the truncation error. Furthermore, the truncation error in TEBD does not necessarily respect conserved quantities, such as the energy and charge, which start deviating from their initial value after a short time scale. This issue can be fixed by using the TDVP method to evolve the state instead. In short, TDVP generates an effective Hamiltonian for the local tensor in MPS, which depends on other tensors. The effective Hamiltonian is used to unitarily evolve the tensor. As a result, the total energy is conserved by construction during the time evolution, and TDVP can take into account other conserved quantities. Although conserved quantity does not necessarily ensure correct local observable, correlation function or transport behavior, this is the first step towards approaching the

corrected non-equilibrium beyond a short time. This is particularly important in the late time regime where hydrodynamics emerges and conserved quantities play an crucial role.

MPS based method – Now, we discuss applying these methods to calculate the OTOC. Like methods using exact diagonalization, one can also calculate OTOC in either the Schrodinger or Heisenberg picture. In Schrodinger’s picture, similar to the exact diagonalization discussed before, the trace in the OTOC $F(t)$ is replaced by an ensemble of states. However, the ensemble of random states is not feasible in the tensor network methods because the random states have large entanglement that MPS cannot capture. Instead, in practice, an ensemble of random product states is used. Fix the initial state as $|\psi\rangle$. Either TEBD or TDVP can be used to generate the following two states,

$$|\psi_1\rangle = e^{iHt} W e^{-iHt} |\psi\rangle, \quad |\psi_2\rangle = \sigma e^{iHt} W e^{-iHt} |\psi\rangle \quad (140)$$

Then the OTOC is just the overlap between the two states followed by averaging over initial states. The two methods, dubbed as TEBD-MPS and TDVP-MPS respectively, which differ by the time evolution method, are compared in detail in [86] and benchmarked with numerical exact Krylov-State method. As expected, the TDVP-MPS method produces more accurate results as time passes a short time scale. Since the numerical cost of TDVP-MPS and TEBD-MPS is comparable, TDVP is the better approach to calculate OTOC in the Schrodinger picture. In the state-based method, the primary source of error is the incapability of representing the complicated state using an MPS with a finite bond dimension.

MPO based method – During the time evolution of a state, the entanglement of the states increases uniformly across the whole system. On the other hand, because of the emergent lightcone structure in the Heisenberg evolution of a local operator shown in Eq. (11), The Heisenberg operator $W(t)$ is almost a product of identity operators $I \otimes \dots \otimes I$ outside the lightcone and becomes complicated inside the lightcone. For this reason, the entanglement entropy of an operator, which can be regarded as a state with doubled physics degree freedom, develops a lightcone profile as well, staying small outside the lightcone and becoming large within the lightcone regardless of the time scale. Therefore, the part of the Heisenberg operator outside the lightcone can be captured accurately using an MPO with a small bond dimension. This intuition leads to the method of calculating OTOC in the Heisenberg picture using MPO. In the MPO-based method, the main step is to evolve the Heisenberg operator, which is similar to evolving MPS by treating the MPO as an MPS with doubled physics degrees of freedom. The time evolution operator to evolve the operator state is

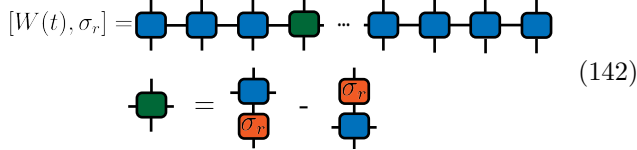
$$W(t) = U W U^\dagger \rightarrow U \otimes U^* |W\rangle \quad (141)$$

This can also be viewed as evolving the operator state $|W\rangle$ using the “super Hamiltonian” $H \otimes I - I \otimes H^*$. The

time evolution can be implemented using either TEBD or TDVP. OTOC can be calculated once MPO form of the Heisenberg operator $W(t)$ is obtained. In this approach, it is more convenient to calculate the OTOC in the form of a squared commutator

$$C(r, t) = \frac{1}{2L} \text{tr}([W(t), \sigma_r]^\dagger [W(t), \sigma_r])$$

where σ_r , a local operator on site r is scanned over the system. Given the MPO of $W(t)$, the MPO of the commutator $[W(t), \sigma_r]$ is obtained efficiently by modifying the local tensor at site r as follows



$$[W(t), \sigma_r] = \text{MPO chain with one green tensor at site } r$$

$$\text{Green tensor} = \text{Blue tensor with red } \sigma_r - \text{Orange tensor with blue } \sigma_r \quad (142)$$

The bond dimension remains the same because σ_r is a local operator. The squared commutator can be obtained by contracting the MPO of the commutator with its Hermitian conjugate copy. However, noticing that $C(r, t)$ is just the square of the Frobenius norm of the commutator, this last step can be replaced by evaluating the norm of the MPO directly by treating it as a MPS. Evaluating the norm of an MPS is a standard tool in the tensor network simulation. Calculating the norm then squaring it is much more accurate than calculating the overlap between the MPO and its Hermitian conjugate copy, especially when $C(r, t)$ is small. Fig. 10(b) shows the squared commutators from the MPO method and the Krylov-State method for 20 qubits. The MPO results is accurate when the squared commutator is small but starts to deviate the exact result from the Krylov-State method as the squared commutator reaches ~ 1 .

As showed in [59], because of the lightcone structure of the Heisenberg operator, the MPO method is very accurate in capturing the tail of OTOC even with a bond dimension as small as 4, and can be used to obtain the butterfly velocity. This method also clearly demonstrates a broadened wavefront, agreeing with the general growth form for $p > 0$, in contrast to the behavior in the SYK chain. Obtaining the asymptotic value of p is quite subtle and requires accessing a wider space-time region and larger bond dimension. The TEBD-MPO method was also compared with TDVP-MPS method in [86], showing both of them are accurate in capturing the tail of OTOC and tracking the lightcone. The TEBD-MPO has two advantages over the TDVP-MPS. First, it does not require sampling over the initial states and thus is free of statistical error. Second, at given time t , the commutator of $W(t)$ and σ_r and therefore $C(r)$ for all r can be obtained efficiently using Eq. (142). On the other hand, in TDVP-MPS method, in order to get $C(r, t)$ for all site r , initial states $\sigma_r |\psi\rangle$ with different r needs to be evolved individually in addition to sample $|\psi\rangle$.

One can also evolve the Heisenberg operator using the TDVP method based on the super-Hamiltonian $H \otimes I -$

$I \otimes H^*$. The quantity made explicitly conserved in the TDVP-MPO method, instead of the energy, is the expectation value of the super Hamiltonian

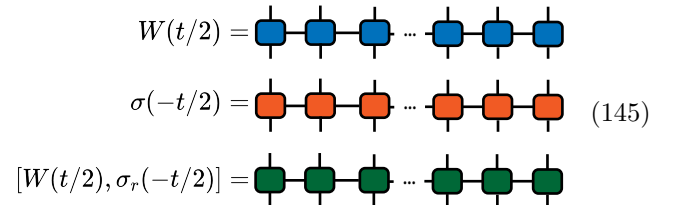
$$\langle W | \mathbb{H} | W \rangle = \text{tr}(W^\dagger(t) H W(t)) - \text{tr}(W(t) H W^\dagger(t)) \quad (143)$$

which is just zero for a Hermitian operator $W(t)$. In practice, TDVP-MPO does not significantly increase the accuracy of TEBD-MPO. It is less accurate to capture the exponentially small value of OTOC because it does not directly take advantage of the lightcone structure. However, TDVP-MPO is still a very useful and convenient method to use when the system has long-range interaction [38], in which case the circuit from Trotterization does not admit the structure shown in Fig. 2. It is also possible to generalize the TDVP-MPO method to conserve energy or/and charge, which remains to be explored.

A few remarks are in order. First, the MPO-based method utilizes the lightcone profile of the entanglement structure of the Heisenberg operator. It becomes exact if the operator entanglement entropy is bounded, such as in the non-interacting system. Second, in a chaotic system, because of the rapid generation of operator entanglement entropy within the lightcone, the tensor network based on the method is not expected to capture the growth and saturation of $C(r, t)$. However, the accuracy of the MPO-based method can be improved significantly with increasing computational cost. The idea is evolving both operators W and σ , forward and backward respectively, and evaluate

$$\frac{1}{2L} \text{tr}([W(t/2), \sigma_r(-t/2)]^\dagger [W(t/2), \sigma_r(-t/2)]). \quad (144)$$

This expression is equivalent to Eq. (142), since $[W(t/2), \sigma_r(-t/2)] = e^{-iHt/2} [W(t), \sigma_r] e^{iHt/2}$. This time-splitting method divides the entanglement growth within the lightcone into two operators and reduces the truncation error. The cost is that each σ_r need to evolved individually in order to obtain the full space-time profile of $C(r, t)$. In addition, the fast construction of the commutator in Eq. (142) is no longer applicable, since now the commutator is between two time evolved Heisenberg operator, both taking MPO form with bond dimension χ . As a result, the MPO of $W(t/2)\sigma(-t/2)$ and $W(t/2)\sigma(-t/2)$ has bond dimension χ^2 , and the MPO of their difference, the commutator, has bond dimension $2\chi^2$. In graphics,



$$W(t/2) = \text{Chain of blue MPO tensors}$$

$$\sigma(-t/2) = \text{Chain of orange MPO tensors}$$

$$[W(t/2), \sigma(-t/2)] = \text{Chain of green MPO tensors} \quad (145)$$

Fixing the physical indices to be α and β , the local tensor of the MPO of the commutator is constructed from the

local tensor of the two Heisenberg operators

$$\begin{aligned}
 \begin{array}{c} \alpha \\ \text{---} \\ \text{[Green Box]} \\ \text{---} \\ \beta \end{array} &= \begin{bmatrix} \begin{array}{c} \alpha \\ \text{---} \\ \text{[Blue Circle]} \\ \text{---} \\ \beta \end{array} & 0 \\ 0 & \begin{array}{c} \alpha \\ \text{---} \\ \text{[Red Circle]} \\ \text{---} \\ \beta \end{array} \end{bmatrix} & \begin{array}{c} \alpha \\ \text{---} \\ \text{[Green Box]} \\ \text{---} \\ \beta \end{array} &= \begin{bmatrix} + & \begin{array}{c} \alpha \\ \text{---} \\ \text{[Blue Circle]} \\ \text{---} \\ \beta \end{array} \\ - & \begin{array}{c} \alpha \\ \text{---} \\ \text{[Red Circle]} \\ \text{---} \\ \beta \end{array} \end{bmatrix} \\
 \begin{array}{c} \alpha \\ \text{---} \\ \text{[Green Box]} \\ \text{---} \\ \beta \end{array} &= \begin{bmatrix} \begin{array}{c} \alpha \\ \text{---} \\ \text{[Blue Circle]} \\ \text{---} \\ \beta \end{array} & \begin{array}{c} \alpha \\ \text{---} \\ \text{[Blue Circle]} \\ \text{---} \\ \beta \end{array} \\ \begin{array}{c} \alpha \\ \text{---} \\ \text{[Red Circle]} \\ \text{---} \\ \beta \end{array} & \begin{array}{c} \alpha \\ \text{---} \\ \text{[Red Circle]} \\ \text{---} \\ \beta \end{array} \end{bmatrix}
 \end{aligned} \tag{146}$$

The minus sign in the local tensor of the last site implements the difference of the two terms in the commutator. Once the MPO of the commutator is constructed, its Frobenius norm and thus the OTOC $C(r, t)$ can be calculated the same as before. As shown in Fig. 10(b), the time splitting approach significantly enhances the accuracy of MPO in the late-time regime. Finally, in all the tensor-network based methods applied to a system with ~ 100 spin, because of the targeted intermediate time scaling $\sim 100/J$, where J is the coupling constant, one should carefully check the convergence of the result with the Trotter time step. In general, the time step dt should be reduced to $\sim 0.005/J$ to avoid accumulating the Trotter error.

VIII. EXPERIMENTAL SCHEMES

As we enter an era of quantum simulation, marked by the existence of multiple experimental platforms with unprecedented power to control and detect quantum many-body physics far from equilibrium, there is a surge of interest in measuring scrambling dynamics and OTOCs. The essential step required to measure an OTOC is to write it as an observable or a combination of observables, including specifying the initial states, the time evolution operators, and the measurements. In this section, we briefly discuss several such experimental schemes, including those already implemented in the laboratory. This discussion focuses on the essence of several OTOC measurement protocols, and it does not delve into the experimental details of various concrete experiments. These schemes fall into two main categories, one requiring rewinding time and the other one requiring measurements averaging over random states.

A. Rewinding time

The experimental schemes falling into this categories requires engineering both forward evolution operator $U(t)$ and backward time evolution operator $U(-t)$, and is closely related to the Loschmidt echo [91]. The first scheme that we describe is based on an interferometric protocol [92]. This scheme requires introducing a reference qubit that is initialized in the state $|+\rangle = \frac{1}{\sqrt{2}}(|0\rangle + |1\rangle)$. The initial state of the system and the

reference qubit is

$$|\Psi_0\rangle = |+\rangle |\psi\rangle. \tag{147}$$

To measure OTOC, one first apply the CNOT gate to the state, controlled by the reference spin, then evolve the state by a butterfly unitary circuit $U_{\text{butterfly}}$, and apply the CNOT gate. The butterfly unitary circuit $U_{\text{butterfly}}$ does not act on the ancillary qubit and is in the following form

$$U_{\text{butterfly}} = U^\dagger(t) W U(t) = W(t) \tag{148}$$

where $U(t)$ is an arbitrary unitary circuit and W is a local unitary gate. The butterfly circuit is just another name for the Heisenberg operator of a local unitary operator. After these steps, the state is

$$\begin{aligned}
 |\Psi\rangle &= \frac{1}{\sqrt{2}} (|0\rangle U_{\text{butterfly}} |\psi\rangle + |1\rangle \sigma_r^x U_{\text{butterfly}} \sigma_r^x |\psi\rangle) \\
 &= \frac{1}{\sqrt{2}} (|0\rangle W(t) |\psi\rangle + |1\rangle \sigma_r^x W(t) \sigma_r^x |\psi\rangle).
 \end{aligned} \tag{149}$$

Given this state, the last step is to measure σ^x on the reference spin. The expectation value, which can be obtained by running the circuit and measuring repetitively, is

$$\langle \Psi | \sigma_r^x | \Psi \rangle = \text{Re} \langle \psi | W^\dagger(t) \sigma_r^x W(t) \sigma_r^x | \psi \rangle \tag{150}$$

in the form of an OTOC. The imaginary part of the OTOC can be obtained by measuring σ^y instead of σ^x . This protocol works for an arbitrary initial state of the system but requires introducing the reference spin and the CNOT gate and is used in [93]

For certain initial states, introducing the reference qubit is not necessary. Consider an initial state that is an eigenstate of a local operator, for instance, σ_r^x . This means that the local qubit of the state is either $|+\rangle$ or $|-\rangle$. The idea is to measure whether the qubit at site r remains an eigenstate of σ_r^x after evolved by the butterfly circuit. This is quantified by its expectation value, given by

$$\langle \psi(t) | \sigma_r^x | \psi(t) \rangle = \langle \psi | W^\dagger(t) \sigma_r^x W(t) | \psi \rangle \tag{151}$$

If the support of $W(t)$ does not overlap site r , then the local qubit remains an eigenstate, otherwise the expectation value decay. Formally, one can write the above equation in the form OTOC $\langle \psi | W^\dagger(t) \sigma_r^x W(t) \sigma_r^x | \psi \rangle$, using the fact that the state $|\psi\rangle$ is an eigenstate of σ_r^x . This scheme is carried out in [94–96]

In the previous example, the OTOC is measured with respect to a pure state. To direct measure OTOC for the infinite temperature ensemble, the most straightforward setup is to prepare double copies of the system, such as a ladder. The initial state is a product of Bell states across each rung $|\Psi\rangle = \prod_i |0\rangle_i |0\rangle_{i'} + |1\rangle_i |1\rangle_{i'}$. The Hamiltonian of the full system $\mathbb{H} = H \otimes I - I \otimes H^*$. Then OTOC can

be cast into an observables in this double copied system

$$\frac{1}{\text{tr}I}(W^\dagger(t)V^\dagger W(t)V) = \langle \Psi | V^\dagger e^{i\mathbb{H}t} W \otimes W^\dagger e^{i\mathbb{H}t} V | \Psi \rangle. \quad (152)$$

Replacing the initial state $|\Psi\rangle$ with the thermal field double state $|\sqrt{\rho}\rangle$ generalizes this scheme to measure OTOC at finite temperature for a specific generalization [97]. The double copy setup is also essential to directly realize the many-body teleportation protocol discussed in Sec. IV, where one copy represents the system and the other copy represents the memory qubit owned by Bob. The many-body teleportation protocol has been implemented in ion trap [98] and superconducting qubits [99] experiments.

It is also possible to measure OTOC at infinite temperature without introducing the second copy in NMR experiments [100–102]. In this setup, the initial state is a high temperature mixed state in the presence of the magnetic field along the z direction. The initial state is given by

$$\rho_0 = \frac{1}{\text{tr}I}(I + \epsilon \sum_r \sigma_r^z). \quad (153)$$

The density matrix is then evolved by unitary time evolution in the form of the butterfly circuit, which can be engineered by a sequence of pulses. In the evolved mixed state, the total magnetization is given by

$$\begin{aligned} \langle \sigma^z \rangle &= \text{tr}(U_\rho(t)\rho_0 U_\rho^\dagger(t)\sigma^z) \\ &= \frac{\epsilon}{\text{tr}I} \text{tr} \left(W(t) \sum_r \sigma_r^z W^\dagger(t) \sum_r \sigma_r^z \right) \end{aligned} \quad (154)$$

in the form of an OTOC. Note that the identity part of the initial mixed state does not contribute to the expectation value. In NMR experiment, a natural choice of W is $\exp(i\theta \sum_r \sigma_r^z)$ from a pulse, which is a non-local operator. Then result $\langle \sigma^z \rangle$ is a periodic function in θ with period 2π , denoted as $\langle \sigma^z \rangle_\theta$. Using the Lehmann representation, one can show that

$$\int_0^{2\pi} d\theta \int d\omega \omega^2 S(\theta) e^{-i\omega\theta} \sim \frac{1}{\text{tr}I} \text{tr}([S^z(t), S^z][S^z(t), S^z]) \quad (155)$$

This squared commutator approximately counts the number of spins within the support of the local Heisenberg operator $\sigma^z(t)$. In practice, one can perform a discrete Fourier transformation on a finite number of measurement results with a discrete value of θ . We note that it is also possible to measure the OTOC between two local operators using selective pulses for an ensemble of small molecules [100].

B. Randomized measurement

The key ingredient for above protocols is the butterfly circuit $U_{\text{butterfly}}$, which requires implementing both $U(t)$

and $U^\dagger(t)$, namely effectively rewinding the time, and can be challenging for generic U . An experimental protocol that bypass this requirement is to exploit statistical correlation from randomized measurement [103], which has been implemented in NMR [104] and ion traps [105]. In its simplest form, this protocol considers the product of two expectation values

$$F(\psi) = \langle \psi | W(t) | \psi \rangle \langle \psi | V^\dagger W(t) V | \psi \rangle \quad (156)$$

When the initial state is averaged over Haar ensemble, using the Haar random average formula in Eq. (A9), the above quantity leads to

$$\begin{aligned} \mathbb{E}_\psi F(\psi) &= \frac{1}{2^N(2^N+1)} \text{tr}(W(t)) \text{tr}(V^\dagger W(t) V) \\ &+ \frac{1}{2^N(2^N+1)} \text{tr}(W(t) V^\dagger W(t) V), \end{aligned} \quad (157)$$

Typically, the first term is $\mathcal{O}(1)$, while the second term, which is the important piece, is $\mathcal{O}(2^{-N})$. However, when W is a traceless operator, the first term vanishes and only the second term, the OTOC, survives. This scheme can also be extended to obtain the leading finite temperature correction of OTOC as well. In this protocol, the major challenge is to prepare the Haar random initial states. Alternatively, one can also estimate the OTOC by sampling over local unitary that acting on each qubit and averaging the initial states in the computational basis in a specific manner. In this approach, the quantity that is being considered is

$$F_{\vec{n}} = \langle \psi_{\vec{n}} | W(t) | \psi_{\vec{n}} \rangle \langle \psi_0 | V^\dagger W(t) V | \psi_0 \rangle. \quad (158)$$

Compared with Eq. (156), the two expectation values are measured from two different states $|\psi_{\vec{n}}\rangle$ and $|\psi_0\rangle$. The state $|\psi_{\vec{n}}\rangle$ are generated by acting local unitary to a state $|n\rangle$ in the computation basis

$$|\psi_{\vec{n}}\rangle = u_1 \otimes \cdots \otimes u_N |\vec{n}\rangle = u_1 |n_1\rangle \otimes u_2 |n_2\rangle \cdots \otimes u_N |n_N\rangle \quad (159)$$

where u_i is drawn from the Haar ensemble or any ensemble that forms 2-design and $n_i \in \{0, 1\}$. The state $|\psi_0\rangle$ is generated from all-zero state $|0\rangle$ using the same unitaries. The random average of the unitaries can be performed independently on each qubit using Eq. (A9). To gain insight on the result, we first average $F_{\vec{n}}$ over u_1 . We define the following operator acting the first qubit

$$\begin{aligned} O_1 &= \langle u_2^{n_2} | \cdots \langle u_N^{n_N} | W(t) | u_2^{n_2} \rangle \cdots | u_N^{n_N} \rangle \\ \tilde{O}_1 &= \langle u_N^0 | \cdots \langle u_2^0 | V^\dagger W(t) V | u_2^0 \rangle \cdots | u_N^0 \rangle \end{aligned} \quad (160)$$

Averaging over u_1 leads to

$$\begin{aligned} \mathbb{E}_{u_1}(F_{\vec{n}}) &= \\ &= \frac{2 - \delta_{n_1,0}}{6} \text{tr}(O_1) \text{tr}(\tilde{O}_1) + \frac{2\delta_{n_1,0} - 1}{6} \text{tr}_{n_1}(O_1 \tilde{O}_1). \end{aligned} \quad (161)$$

The trick here is to use a weighted sum over n_1 to cancel the first term. One can show that

$$\sum_{n_1} \left(-\frac{1}{2}\right)^{n_1} \mathbb{E}_{u_1} F_{\vec{n}} = \frac{1}{4} \text{tr}(O_1 \tilde{O}_1). \quad (162)$$

Consecutively averaging over other local unitaries u_i and summing over n_i in the similar fashion leads to the OTOC

$$\sum_{\vec{n}} \left(-\frac{1}{2}\right)^{\sum n_i} \mathbb{E}_{u_1, \dots, u_N} (F_{\vec{n}}) = \frac{1}{4^N} \text{tr}(W(t) V^\dagger W(t) V). \quad (163)$$

One can also extend this protocol to directly measure the operator probability distribution defined in Sec. V [106].

IX. EPILOGUE

In this tutorial, we covered the definition of quantum scrambling dynamics in generic quantum many-body systems, how to probe the information dynamics, and how to recover the information when it is fully scrambled in the system. We demonstrated the important role of OTOCs in quantum information and dynamics and discussed their general behavior in local systems featuring ballistic information dynamics. We presented several toy models where the OTOC can be calculated exactly as well as numerical tools to compute OTOCs in generic systems. We also surveyed recent exciting experimental progress in detecting information dynamics. However, it is not practical to cover all the aspects of this large field in this tutorial article. There are several related interesting topics that we did not talk about and would like to briefly mention here.

Finite temperature – First, this tutorial largely considered scrambling at infinite temperature. Physically, this amounts to saying that Alice and Bob were using a medium at high temperature compared to the scales in the intrinsic Hamiltonian. Mathematically, this means we considered OTOCs where the expectation was taken in the maximally mixed state. This regime is ideal for understanding the basics of information dynamics since we do not have to deal with any static correlations in the quantum state. It is also the most relevant regime for current experiments. However, it is interesting to understand information away from infinite temperature, especially in the context of black hole physics.

Given a quantum state ρ , one can define an OTOC in this state by $F_\rho = \text{tr}(\rho W(t) V W(t) V)$. When ρ is the maximally mixed state, this recovers the simple trace expression we considered for most of this tutorial. However, if Alice and Bob wish to use a medium at non-infinite temperature to convey quantum information, then one expects so-called thermal OTOCs to be relevant where $\rho \propto e^{-\beta H}$ is a thermal equilibrium state. However, the physics of scrambling is more complicated in this case. This is because there are multiple versions of F_ρ called

“regulated” OTOCs,

$$\tilde{F}_\rho = \text{tr}(\rho^{q_1} W(t) \rho^{q_2} V \rho^{q_3} W(t) \rho^{q_4} V), \quad (164)$$

where $q_i \in [0, 1]$ and $\sum_i q_i = 1$. This class of objects corresponds to displacing the operators $W(t)$ and V in imaginary time (when $\rho \propto e^{-\beta H}$ is the thermal state).

The case $q_1 = 1, q_{i>1} = 0$ is the usual OTOC in state ρ . The case $q_i = 1/4$ is a particularly natural choice from a mathematical point of view; this is the form of OTOC to which the MSS bound [11] applies. In early examples, these different regularizations gave equivalent characterizations of the scrambling dynamics. However, it was later discovered that the butterfly velocity can depend on the choice of regularization [107–109]. This raises the question of which regularization is most relevant for information spreading. A finite temperature version of some of our information calculations was given in an appendix of [12]. A notion of “perfect size winding” [110] has also been shown to be related to optimal many-body teleportation at finite temperature. Both of these cases are related to the $(1/2, 0, 1/2, 0)$ and $(1/4, 1/4, 1/4, 1/4)$ OTOCs, but there is still work to do to elucidate the general structure of information spreading at finite temperature. There are several proposals to measure OTOC at finite temperature for different regularization [97, 103, 111], and recently OTOC with regularization $(1/2, 0, 0, 1/2)$ is measured experimentally in a small system [112].

Symmetries – Symmetries and conservation laws can strongly affect scrambling dynamics. The basic intuition is that a initial state cannot scramble as much in the presence of conserved quantities due to the restricted Hilbert space. For instance, the early growth rate of OTOC is suppressed by temperature [11] and/or chemical potentials [113, 114]. Moreover, in extended systems, conserved quantities usually lead to slow mode associated with their transport, which can significantly slow down the scrambling dynamics and cause a prolong power-law tail of OTOC in the late time regime [44, 74–76, 115].

An interesting question regarding symmetry is how it affects the information recover fidelity in the Hayden-Preskill protocol discussed in Sec. IV. It boils down to study the late-time value of OTOC appearing in Eq. (71), which we repeat here

$$F_{\text{EPR}} = \left(\frac{1}{4^{|E|}} \frac{1}{2^N} \sum_{W_1, V_E} \text{tr}(W_1(-t) V_E W_1(-t) V_E) \right)^{-1}, \quad (165)$$

where $W(-t) = U W U^\dagger$. This equation holds for any unitary operator U acting on qubit systems. In the presence of conserved quantity Q , we have $[U, Q] = 0$. Due to the block diagonalized structure U , the late value of OTOCs cannot be estimated using Haar random unitary such as in Eq. (83). Instead of scaling with $1/2^N$, one can show that in systems with conserved charge or energy, the late-time value of the OTOCs scale as $\mathcal{O}(1/\text{poly}(N))$ [114, 116]. Larger symmetry group can

even leads to finite late value of OTOCs and thus significantly suppress the recovery fidelity [117, 118].

More on wavefront broadening – Another direction concerns conjectured universality in the OTOC structure in locally interacting systems. In Section VI we indicated that semi-classical/large N models and random circuit models gave two distinct classes of OTOC behavior, and we argued that the random circuit behavior was generic, i.e. that finite N corrections would qualitatively change the large N form of the OTOC. It is important to understand better the universality classes that can arise, especially in Hamiltonian systems at non-infinite temperature. In the literature, OTOCs are sometimes analyzed along a ray within the lightcone in terms of a velocity-dependent Lyapunov exponent [65, 119],

$$C(x, t) \sim e^{\lambda(v)t}, \quad (166)$$

where $v = |x|/t$. For instance, $\lambda(v) = \lambda(1 - v/v_B)^{p+1}$ for the growth form in Eq. (94). The definition of the butterfly velocity is $\lambda(v_B) = 0$, and at large N one typically finds that $\partial_v \lambda(v)|_{v_B} \neq 0$. This corresponds to $p = 0$ in our discussion above. By contrast, the 1d random circuit form has $\partial_v \lambda(v)|_{v_B} = 0$, which corresponds to $p = 1$. As we said, the latter form is conjectured to be generic in 1d, but it is important to better understand this issue.

Quantum chaos – Another motivation of studying OTOCs in the literature lies in its connection to quantum chaos. In the semi-classical regime, schematically, one can replace the commutator in the squared commutator with a Poisson bracket and obtain [19, 120]

$$C = \frac{1}{\text{tr} I} \text{tr}([x(t), p]^2) \approx \{x(t), p\}^2 = \left(\frac{\partial x(t)}{\partial x} \right)^2 \quad (167)$$

which measures the sensitivity of the final position to the initial position, and thus classical chaos. Then it seems natural to promote the squared commutator to be a diagnosis of quantum chaos [11]. However, it turns out to be quite subtle [121]. For instance, although C is expected to exhibit early time Lyapunov growth in the semi-classical limit of many-body system before saturation [120, 122], not all quantum many-body systems have a semi-classical limit. The squared commutator of the unitary random circuit model does not have the exponential growth behavior expected to be a diagnosis of quantum many-body chaos. On the other hand, some integrable systems exhibits early time exponential growth due to unstable dynamics [123, 124]. Therefore while the late-time value of OTOC has a clear physics meaning as discussed in Sec. V, the connection of the early-time growth of the squared commutator to previous proposed measures of quantum many-body chaos (see [125, 126] for discussions), such as the spectrum form factor from the random matrix behavior, needs to be further settled. A more general question is whether quantum scrambling and quantum many-body chaos measure the same property, and if not, when they differ from each other.

More on numerical methods – Ongoing experiments on scrambling and non-equilibrium quantum many-body

dynamics in general are reaching system sizes beyond the capability of exact diagonalization, calling for new numerical tools. In Sec. VII, we discussed an MPO/MPS-based method to calculate the tail of OTOCs for large system size in 1D utilizing the lightcone structure of operator spreading. One direction is to extend such a method to higher dimension using other ansatz for states or operators.

Moreover, it would be ideal to develop general purpose numerical tools to directly simulate many-body teleportation for arbitrary unitary circuit with local structure and initial states for large system size of ~ 100 qubits. The conventional MPS/MPO based method does not work due to the rapid growth of the entanglement entropy that an MPS with a finite bond dimension cannot capture. It would be interesting to explore the effectiveness of other wavefunction ansatz, such as various neural network states or multi-scale entanglement renormalization ansatz (MERA), in this context. For example, [127] calculates the OTOCs of the mixed field Ising model in 2D using the restricted Boltzmann machine.

Understanding scrambling dynamics, i.e., how information flows from local to non-local degrees of freedom, is also useful for developing numerical method to simulate conventional thermalization dynamics of local observables and calculate transport coefficient, which is usually given time ordered two-point correlation function. Schematically, in strongly interacting system, the equation of motion of single qubit observable depends on the equation of motion of two-qubit observable, which depends on three-qubit observables, leading to an infinite series of equations involving arbitrary order of correlations functions that becomes impractical to solve. Given transport is captured by low order correlations. It is tempting to assume the dynamics of sufficiently high order correlation functions does not feedback to the dynamics of simple correlation functions and to truncate the infinite series of equations or simplify the higher order equations by approximation. These ideas have led to multiple new numerical algorithms [128–132]. There is still work to do to justify the assumptions and better understand the interplay between the scrambling dynamics and dynamics of local observables.

We believe that we are only just starting to explore this exciting field of quantum information scrambling. With the many connections discovered so far and the prospect of new large-scale experiments on the horizon, there are many exciting possibilities to explore including the discovery of new maximally chaotic quantum systems, the laboratory simulation of holographic models of quantum gravity, a deeper understanding of quantum chaos, new insights into transport in strongly interacting systems, and much else. We therefore hope that the reader will consider getting into this field and bringing a new point of view.

X. ACKNOWLEDGEMENT

S.X thanks the hospitality of the KITP supported by the National Science Foundation under Grant No. NSF PHY-1748958, and S.X. and B.G.S. thank the hospitality of the Aspen Center for Physics supported by National Science Foundation grant PHY-1607611, where part of

the tutorial was written. The numerical simulations in this tutorial were conducted with the advanced computing resources provided by Texas A&M High Performance Research Computing. BGS thanks the organizers and participants of the 2018 Boulder Summer School on Quantum Information where some of the material discussed here was presented.

-
- [1] E. Altman, K. R. Brown, G. Carleo, L. D. Carr, E. Demler, C. Chin, B. DeMarco, S. E. Economou, M. A. Eriksson, K.-M. C. Fu, *et al.*, Quantum simulators: Architectures and opportunities, [PRX Quantum](#) **2**, 017003 (2021).
 - [2] J. M. Deutsch, Quantum statistical mechanics in a closed system, [Physical Review A](#) **43**, 2046 (1991).
 - [3] M. Srednicki, Chaos and quantum thermalization, [Physical Review E](#) **50**, 888 (1994).
 - [4] M. Rigol, V. Dunjko, and M. Olshanii, Thermalization and its mechanism for generic isolated quantum systems, [Nature](#) **452**, 854 (2008).
 - [5] A. Polkovnikov, K. Sengupta, A. Silva, and M. Vengalattore, Colloquium: Nonequilibrium dynamics of closed interacting quantum systems, [Reviews of Modern Physics](#) **83**, 863 (2011).
 - [6] A. M. Kaufman, M. E. Tai, A. Lukin, M. Rispoli, R. Schittko, P. M. Preiss, and M. Greiner, Quantum thermalization through entanglement in an isolated many-body system, [Science](#) **353**, 794 (2016).
 - [7] P. Hayden and J. Preskill, Black holes as mirrors: quantum information in random subsystems, [J. High Energy Phys](#) **2007**, 120 (2007).
 - [8] Y. Sekino and L. Susskind, Fast scramblers, [J. High Energy Phys](#) **2008**, 065 (2008).
 - [9] S. H. Shenker and D. Stanford, Black holes and the butterfly effect, [J. High Energy Phys](#) **2014**, 1 (2014).
 - [10] S. H. Shenker and D. Stanford, Stringy effects in scrambling, [J. High Energy Phys](#) **2015**, 1 (2015).
 - [11] J. Maldacena, S. H. Shenker, and D. Stanford, A bound on chaos, [J. High Energy Phys](#) **2016**, 1 (2016).
 - [12] P. Hosur, X.-L. Qi, D. A. Roberts, and B. Yoshida, Chaos in quantum channels, [J. High Energy Phys](#) **2016**, 1 (2016).
 - [13] D. A. Roberts and B. Yoshida, Chaos and complexity by design, [J. High Energy Phys](#) **2017**, 1 (2017).
 - [14] B. Swingle, Unscrambling the physics of out-of-time-order correlators, [Nature Physics](#) **14**, 988 (2018).
 - [15] R. Lewis-Swan, A. Safavi-Naini, A. Kaufman, and A. Rey, Dynamics of quantum information, [Nature Reviews Physics](#) **1**, 627 (2019).
 - [16] E. H. Lieb and D. W. Robinson, The finite group velocity of quantum spin systems, in *Statistical mechanics* (Springer, 1972) pp. 425–431.
 - [17] H. Liu and S. J. Suh, Entanglement tsunami: universal scaling in holographic thermalization, [Physical Review Letters](#) **112**, 011601 (2014).
 - [18] E. Iyoda and T. Sagawa, Scrambling of quantum information in quantum many-body systems, [Physical Review A](#) **97**, 042330 (2018).
 - [19] A. Larkin and Y. N. Ovchinnikov, Quasiclassical method in the theory of superconductivity, [Sov Phys JETP](#) **28**, 1200 (1969).
 - [20] B. Yoshida and A. Kitaev, Efficient decoding for the hayden-preskill protocol, [arXiv preprint arXiv:1710.03363](#) (2017).
 - [21] A. R. Brown, H. Gharibyan, S. Leichenauer, H. W. Lin, S. Nezami, G. Salton, L. Susskind, B. Swingle, and M. Walter, Quantum gravity in the lab: teleportation by size and traversable wormholes, [arXiv preprint arXiv:1911.06314](#) (2019).
 - [22] T. Schuster, B. Kobrin, P. Gao, I. Cong, E. T. Khabiboulline, N. M. Linke, M. D. Lukin, C. Monroe, B. Yoshida, and N. Y. Yao, Many-body quantum teleportation via operator spreading in the traversable wormhole protocol, [arXiv preprint arXiv:2102.00010](#) (2021).
 - [23] B. Yoshida and N. Y. Yao, Disentangling scrambling and decoherence via quantum teleportation, [Physical Review X](#) **9**, 011006 (2019).
 - [24] B. Yan and N. A. Sinitsyn, Recovery of damaged information and the out-of-time-ordered correlators, [Physical Review Letters](#) **125**, 040605 (2020).
 - [25] X.-L. Qi and A. Streicher, Quantum epidemiology: operator growth, thermal effects, and syk, [Journal of High Energy Physics](#) **2019**, 1 (2019).
 - [26] D. E. Parker, X. Cao, A. Avdoshkin, T. Scaffidi, and E. Altman, A universal operator growth hypothesis, [Physical Review X](#) **9**, 041017 (2019).
 - [27] A. Periwal, E. S. Cooper, P. Kunkel, J. F. Wienand, E. J. Davis, and M. Schleier-Smith, Programmable interactions and emergent geometry in an array of atom clouds, [Nature](#) **600**, 630 (2021).
 - [28] N. Lashkari, D. Stanford, M. Hastings, T. Osborne, and P. Hayden, Towards the fast scrambling conjecture, [J. High Energy Phys](#) **2013**, 1 (2013).
 - [29] M. Blake, H. Lee, and H. Liu, A quantum hydrodynamical description for scrambling and many-body chaos, [Journal of High Energy Physics](#) **2018**, 1 (2018).
 - [30] C. Murthy and M. Srednicki, Bounds on chaos from the eigenstate thermalization hypothesis, [Physical review letters](#) **123**, 230606 (2019).
 - [31] A. Chan, A. De Luca, and J. Chalker, Eigenstate correlations, thermalization, and the butterfly effect, [Physical Review Letters](#) **122**, 220601 (2019).
 - [32] S. Pappalardi, L. Foini, and J. Kurchan, Quantum bounds and fluctuation-dissipation relations, [arXiv preprint arXiv:2110.03497](#) (2021).
 - [33] G. Bentsen, Y. Gu, and A. Lucas, Fast scrambling on sparse graphs, [Proceedings of the National Academy of Sciences](#) **116**, 6689 (2019).
 - [34] G. Bentsen, T. Hashizume, A. S. Buyskikh, E. J. Davis, A. J. Daley, S. S. Gubser, and M. Schleier-Smith, Tree-like interactions and fast scrambling with cold atoms,

- Physical Review Letters **123**, 130601 (2019).
- [35] A. W. Harrow, L. Kong, Z.-W. Liu, S. Mehraban, and P. W. Shor, Separation of out-of-time-ordered correlation and entanglement, *PRX Quantum* **2**, 020339 (2021).
 - [36] T. Kuwahara and K. Saito, Absence of fast scrambling in thermodynamically stable long-range interacting systems, *Physical Review Letters* **126**, 030604 (2021).
 - [37] X. Chen and T. Zhou, Quantum chaos dynamics in long-range power law interaction systems, *Physical Review B* **100**, 064305 (2019).
 - [38] T. Zhou, S. Xu, X. Chen, A. Guo, and B. Swingle, Operator lévy flight: Light cones in chaotic long-range interacting systems, *Physical Review Letters* **124**, 180601 (2020).
 - [39] C.-F. Chen and A. Lucas, Finite speed of quantum scrambling with long range interactions, *Physical Review Letters* **123**, 250605 (2019).
 - [40] T. Kuwahara and K. Saito, Strictly linear light cones in long-range interacting systems of arbitrary dimensions, *Physical Review X* **10**, 031010 (2020).
 - [41] M. C. Tran, C.-F. Chen, A. Ehrenberg, A. Y. Guo, A. Deshpande, Y. Hong, Z.-X. Gong, A. V. Gorshkov, and A. Lucas, Hierarchy of linear light cones with long-range interactions, *Physical Review X* **10**, 031009 (2020).
 - [42] Y. Chen, Universal logarithmic scrambling in many body localization, *arXiv preprint arXiv:1608.02765* (2016).
 - [43] R. Fan, P. Zhang, H. Shen, and H. Zhai, Out-of-time-order correlation for many-body localization, *Science bulletin* **62**, 707 (2017).
 - [44] X. Chen, T. Zhou, D. A. Huse, and E. Fradkin, Out-of-time-order correlations in many-body localized and thermal phases, *Annalen der Physik* **529**, 1600332 (2017).
 - [45] K. Slagle, Z. Bi, Y.-Z. You, and C. Xu, Out-of-time-order correlation in marginal many-body localized systems, *Physical Review B* **95**, 165136 (2017).
 - [46] Y. Huang, Y.-L. Zhang, and X. Chen, Out-of-time-ordered correlators in many-body localized systems, *Annalen der Physik* **529**, 1600318 (2017).
 - [47] B. Swingle and D. Chowdhury, Slow scrambling in disordered quantum systems, *Physical Review B* **95**, 060201 (2017).
 - [48] A. Nahum, J. Ruhman, and D. A. Huse, Dynamics of entanglement and transport in one-dimensional systems with quenched randomness, *Physical Review B* **98**, 035118 (2018).
 - [49] S. Sahu, S. Xu, and B. Swingle, Scrambling dynamics across a thermalization-localization quantum phase transition, *Physical Review Letters* **123**, 165902 (2019).
 - [50] A. Smith, J. Knolle, R. Moessner, and D. L. Kovrizhin, Logarithmic spreading of out-of-time-ordered correlators without many-body localization, *Physical Review Letters* **123**, 086602 (2019).
 - [51] J. Feldmeier and M. Knap, Critically slow operator dynamics in constrained many-body systems, *Physical Review Letters* **127**, 235301 (2021).
 - [52] S. Xu, X. Li, Y.-T. Hsu, B. Swingle, and S. D. Sarma, Butterfly effect in interacting aubry-andre model: thermalization, slow scrambling, and many-body localization, *Physical Review Research* **1**, 032039 (2019).
 - [53] F. S. Lozano-Negro, P. R. Zangara, and H. M. Pastawski, Ergodicity breaking in an incommensurate system observed by otocs and loschmidt echoes: From quantum diffusion to sub-diffusion, *Chaos, Solitons & Fractals* **150**, 111175 (2021).
 - [54] I. L. Aleiner, L. Faoro, and L. B. Ioffe, Microscopic model of quantum butterfly effect: out-of-time-order correlators and traveling combustion waves, *Annals of Physics* **375**, 378 (2016).
 - [55] D. A. Roberts and B. Swingle, Lieb-robinson bound and the butterfly effect in quantum field theories, *Physical Review Letters* **117**, 091602 (2016).
 - [56] C.-J. Lin and O. I. Motrunich, Out-of-time-ordered correlators in a quantum ising chain, *Physical Review B* **97**, 144304 (2018).
 - [57] S. Gopalakrishnan, D. A. Huse, V. Khemani, and R. Vasseur, Hydrodynamics of operator spreading and quasiparticle diffusion in interacting integrable systems, *Physical Review B* **98**, 220303 (2018).
 - [58] A. Bohrdt, C. B. Mendl, M. Endres, and M. Knap, Scrambling and thermalization in a diffusive quantum many-body system, *New Journal of Physics* **19**, 063001 (2017).
 - [59] S. Xu and B. Swingle, Accessing scrambling using matrix product operators, *Nature Physics* **16**, 199 (2020).
 - [60] A. Nahum, S. Vijay, and J. Haah, Operator spreading in random unitary circuits, *Physical Review X* **8**, 021014 (2018).
 - [61] C. Von Keyserlingk, T. Rakovszky, F. Pollmann, and S. L. Sondhi, Operator hydrodynamics, otocs, and entanglement growth in systems without conservation laws, *Physical Review X* **8**, 021013 (2018).
 - [62] A. Chan, A. De Luca, and J. Chalker, Solution of a minimal model for many-body quantum chaos, *Physical Review X* **8**, 041019 (2018).
 - [63] B. Bertini and L. Piroli, Scrambling in random unitary circuits: Exact results, *Physical Review B* **102**, 064305 (2020).
 - [64] Y. Gu, X.-L. Qi, and D. Stanford, Local criticality, diffusion and chaos in generalized sachdev-ye-kitaev models, *J. High Energy Phys* **2017**, 1 (2017).
 - [65] V. Khemani, D. A. Huse, and A. Nahum, Velocity-dependent lyapunov exponents in many-body quantum, semiclassical, and classical chaos, *Physical Review B* **98**, 144304 (2018).
 - [66] S. Sachdev and J. Ye, Gapless spin-fluid ground state in a random quantum Heisenberg magnet, *Phys. Rev. Lett.* **70**, 3339 (1993).
 - [67] A. Kitaev, A simple model of quantum holography, in *KITP Program: Entanglement in Strongly-Correlated Quantum Matter* (2015).
 - [68] D. Chowdhury, A. Georges, O. Parcollet, and S. Sachdev, Sachdev-ye-kitaev models and beyond: A window into non-fermi liquids, *arXiv preprint arXiv:2109.05037* (2021).
 - [69] D. Ben-Zion and J. McGreevy, Strange metal from local quantum chaos, *Physical Review B* **97**, 155117 (2018).
 - [70] Z. Bi, C.-M. Jian, Y.-Z. You, K. A. Pawlak, and C. Xu, Instability of the non-fermi-liquid state of the sachdev-ye-kitaev model, *Physical Review B* **95**, 205105 (2017).
 - [71] S.-K. Jian and H. Yao, Solvable sachdev-ye-kitaev models in higher dimensions: from diffusion to many-body localization, *Physical Review Letters* **119**, 206602 (2017).

- [72] Y. Gu and A. Kitaev, On the relation between the magnitude and exponent of otocs, *J. High Energy Phys* **2019**, 1 (2019).
- [73] A. Nahum, J. Ruhman, S. Vijay, and J. Haah, Quantum entanglement growth under random unitary dynamics, *Physical Review X* **7**, 031016 (2017).
- [74] T. Rakovszky, F. Pollmann, and C. Von Keyserlingk, Diffusive hydrodynamics of out-of-time-ordered correlators with charge conservation, *Physical Review X* **8**, 031058 (2018).
- [75] V. Khemani, A. Vishwanath, and D. A. Huse, Operator spreading and the emergence of dissipative hydrodynamics under unitary evolution with conservation laws, *Physical Review X* **8**, 031057 (2018).
- [76] S. Pai, M. Pretko, and R. M. Nandkishore, Localization in fractonic random circuits, *Physical Review X* **9**, 021003 (2019).
- [77] P. Saad, S. H. Shenker, and D. Stanford, A semiclassical ramp in syk and in gravity, *arXiv preprint arXiv:1806.06840* (2018).
- [78] S. Xu and B. Swingle, Locality, quantum fluctuations, and scrambling, *Physical Review X* **9**, 031048 (2019).
- [79] T. Zhou and X. Chen, Operator dynamics in a brownian quantum circuit, *Physical Review E* **99**, 052212 (2019).
- [80] C. Sünderhauf, L. Piroli, X.-L. Qi, N. Schuch, and J. I. Cirac, Quantum chaos in the brownian syk model with large finite n : Otc and tripartite information, *J. High Energy Phys* **2019**, 1 (2019).
- [81] S.-K. Jian and B. Swingle, Note on entropy dynamics in the brownian syk model, *J. High Energy Phys* **2021**, 1 (2021).
- [82] E. Brunet, B. Derrida, A. Mueller, and S. Munier, Phenomenological theory giving the full statistics of the position of fluctuating pulled fronts, *Physical Review E* **73**, 056126 (2006).
- [83] A. Keselman, L. Nie, and E. Berg, Scrambling and lyapunov exponent in spatially extended systems, *Physical Review B* **103**, L121111 (2021).
- [84] D. J. Luitz and Y. B. Lev, Information propagation in isolated quantum systems, *Physical Review B* **96**, 020406 (2017).
- [85] B. Kobrin, Z. Yang, G. D. Kahanamoku-Meyer, C. T. Olund, J. E. Moore, D. Stanford, and N. Y. Yao, Many-body chaos in the sachdev-ye-kitaev model, *Physical Review Letters* **126**, 030602 (2021).
- [86] K. Hémerly, F. Pollmann, and D. J. Luitz, Matrix product states approaches to operator spreading in ergodic quantum systems, *Physical Review B* **100**, 104303 (2019).
- [87] J. Lopez-Piqueres, B. Ware, S. Gopalakrishnan, and R. Vasseur, Operator front broadening in chaotic and integrable quantum chains, *Physical Review B* **104**, 104307 (2021).
- [88] D. Yuan, S.-Y. Zhang, Y. Wang, L.-M. Duan, and D.-L. Deng, Quantum information scrambling in quantum many-body scarred systems, *arXiv preprint arXiv:2201.01777* (2022).
- [89] S. Paeckel, T. Köhler, A. Swoboda, S. R. Manmana, U. Schollwöck, and C. Hubig, Time-evolution methods for matrix-product states, *Annals of Physics* **411**, 167998 (2019).
- [90] U. Schollwöck, The density-matrix renormalization group in the age of matrix product states, *Annals of physics* **326**, 96 (2011).
- [91] B. Yan, L. Cincio, and W. H. Zurek, Information scrambling and loschmidt echo, *Physical Review Letters* **124**, 160603 (2020).
- [92] B. Swingle, G. Bentsen, M. Schleier-Smith, and P. Hayden, Measuring the scrambling of quantum information, *Physical Review A* **94**, 040302 (2016).
- [93] X. Mi, P. Roushan, C. Quintana, S. Mandrà, J. Marshall, C. Neill, F. Arute, K. Arya, J. Atalaya, R. Babush, *et al.*, Information scrambling in quantum circuits, *Science* **374**, 1479 (2021).
- [94] M. Gärttner, J. G. Bohnet, A. Safavi-Naini, M. L. Wall, J. J. Bollinger, and A. M. Rey, Measuring out-of-time-order correlations and multiple quantum spectra in a trapped-ion quantum magnet, *Nature Physics* **13**, 781 (2017).
- [95] J. Braumüller, A. H. Karamlou, Y. Yanay, B. Kannan, D. Kim, M. Kjaergaard, A. Melville, B. M. Niedzielski, Y. Sung, A. Vepsäläinen, *et al.*, Probing quantum information propagation with out-of-time-ordered correlators, *Nature Physics* , 1 (2021).
- [96] S. Zhao, Z.-Y. Ge, Z. Xiang, G. Xue, H. Yan, Z. Wang, Z. Wang, H. Xu, F. Su, Z. Yang, *et al.*, Probing operator spreading via floquet engineering in a superconducting circuit, *arXiv preprint arXiv:2108.01276* (2021).
- [97] B. Sundar, A. Elben, L. K. Joshi, and T. V. Zache, Proposal for measuring out-of-time-ordered correlators at finite temperature with coupled spin chains, *New Journal of Physics* (2022).
- [98] K. A. Landsman, C. Figgatt, T. Schuster, N. M. Linke, B. Yoshida, N. Y. Yao, and C. Monroe, Verified quantum information scrambling, *Nature* **567**, 61 (2019).
- [99] J.-H. Wang, T.-Q. Cai, X.-Y. Han, Y.-W. Ma, Z.-L. Wang, Z.-H. Bao, Y. Li, H.-Y. Wang, H.-Y. Zhang, L.-Y. Sun, *et al.*, Verifying quantum information scrambling dynamics in a fully controllable superconducting quantum simulator, *arXiv preprint arXiv:2112.11204* (2021).
- [100] J. Li, R. Fan, H. Wang, B. Ye, B. Zeng, H. Zhai, X. Peng, and J. Du, Measuring out-of-time-order correlators on a nuclear magnetic resonance quantum simulator, *Physical Review X* **7**, 031011 (2017).
- [101] K. X. Wei, C. Ramanathan, and P. Cappellaro, Exploring localization in nuclear spin chains, *Physical Review Letters* **120**, 070501 (2018).
- [102] C. Sánchez, A. Chattah, K. Wei, L. Buljubasich, P. Cappellaro, and H. Pastawski, Perturbation independent decay of the loschmidt echo in a many-body system, *Physical Review Letters* **124**, 030601 (2020).
- [103] B. Vermersch, A. Elben, L. M. Sieberer, N. Y. Yao, and P. Zoller, Probing scrambling using statistical correlations between randomized measurements, *Physical Review X* **9**, 021061 (2019).
- [104] X. Nie, Z. Zhang, X. Zhao, T. Xin, D. Lu, and J. Li, Detecting scrambling via statistical correlations between randomized measurements on an nmr quantum simulator, *arXiv preprint arXiv:1903.12237* (2019).
- [105] M. K. Joshi, A. Elben, B. Vermersch, T. Brydges, C. Maier, P. Zoller, R. Blatt, and C. F. Roos, Quantum information scrambling in a trapped-ion quantum simulator with tunable range interactions, *Physical Review Letters* **124**, 240505 (2020).
- [106] X.-L. Qi, E. J. Davis, A. Periwal, and M. Schleier-Smith, Measuring operator size growth in quantum quench experiments, *arXiv preprint arXiv:1906.00524* (2019).

- [107] Y. Liao and V. Galitski, Nonlinear sigma model approach to many-body quantum chaos: Regularized and unregularized out-of-time-ordered correlators, *Physical Review B* **98**, 205124 (2018).
- [108] S. Sahu and B. Swingle, Information scrambling at finite temperature in local quantum systems, *Physical Review B* **102**, 184303 (2020).
- [109] A. Romero-Bermúdez, K. Schalm, and V. Scopelliti, Regularization dependence of the otoc. which lyapunov spectrum is the physical one?, *Journal of High Energy Physics* **2019**, 1 (2019).
- [110] S. Nezami, H. W. Lin, A. R. Brown, H. Gharibyan, S. Leichenauer, G. Salton, L. Susskind, B. Swingle, and M. Walter, Quantum gravity in the lab: teleportation by size and traversable wormholes, part ii, *arXiv preprint arXiv:2102.01064* (2021).
- [111] N. Y. Yao, F. Grusdt, B. Swingle, M. D. Lukin, D. M. Stamper-Kurn, J. E. Moore, and E. A. Demler, Interferometric approach to probing fast scrambling, *arXiv preprint arXiv:1607.01801* (2016).
- [112] A. M. Green, A. Elben, C. H. Alderete, L. K. Joshi, N. H. Nguyen, T. V. Zache, Y. Zhu, B. Sundar, and N. M. Linke, Experimental measurement of out-of-time-ordered correlators at finite temperature, *arXiv preprint arXiv:2112.02068* (2021).
- [113] X. Chen, Y. Gu, and A. Lucas, Many-body quantum dynamics slows down at low density, *SciPost Physics* **9**, 071 (2020).
- [114] L. Agarwal and S. Xu, Emergent symmetry in brownian syk models and charge dependent scrambling, *arXiv preprint arXiv:2108.05810* (2021).
- [115] G. Cheng and B. Swingle, Scrambling with conservation laws, *Journal of High Energy Physics* **2021**, 1 (2021).
- [116] Y. Huang, F. G. Brandao, Y.-L. Zhang, *et al.*, Finite-size scaling of out-of-time-ordered correlators at late times, *Physical Review Letters* **123**, 010601 (2019).
- [117] J. Kudler-Flam, R. Sohal, and L. Nie, Information scrambling with conservation laws, *arXiv preprint arXiv:2107.04043* (2021).
- [118] H. Tajima and K. Saito, Universal limitation of quantum information recovery: symmetry versus coherence, *arXiv preprint arXiv:2103.01876* (2021).
- [119] M. Mezei and G. Sárosi, Chaos in the butterfly cone, *Journal of High Energy Physics* **2020**, 1 (2020).
- [120] E. B. Rozenbaum, S. Ganesan, and V. Galitski, Lyapunov exponent and out-of-time-ordered correlator's growth rate in a chaotic system, *Physical Review Letters* **118**, 086801 (2017).
- [121] I. Kukuljan, S. Grozdanov, and T. Prosen, Weak quantum chaos, *Physical Review B* **96**, 060301 (2017).
- [122] J. Rammensee, J. D. Urbina, and K. Richter, Many-body quantum interference and the saturation of out-of-time-order correlators, *Physical Review Letters* **121**, 124101 (2018).
- [123] Q. Hummel, B. Geiger, J. D. Urbina, and K. Richter, Reversible quantum information spreading in many-body systems near criticality, *Physical review letters* **123**, 160401 (2019).
- [124] T. Xu, T. Scaffidi, and X. Cao, Does scrambling equal chaos?, *Physical Review Letters* **124**, 140602 (2020).
- [125] B. Arpan, C. Wissam, H. S. Shajidul, and B. Yan, Towards the web of quantum chaos diagnostics, *The European Physical Journal. C, Particles and Fields*. **82** (2022).
- [126] J. Kudler-Flam, L. Nie, and S. Ryu, Conformal field theory and the web of quantum chaos diagnostics, *Journal of High Energy Physics* **2020**, 1 (2020).
- [127] Y. Wu, L.-M. Duan, and D.-L. Deng, Artificial neural network based computation for out-of-time-ordered correlators, *Physical Review B* **101**, 214308 (2020).
- [128] E. Leviatan, F. Pollmann, J. H. Bardarson, D. A. Huse, and E. Altman, Quantum thermalization dynamics with matrix-product states, *arXiv preprint arXiv:1702.08894* (2017).
- [129] C. D. White, M. Zaletel, R. S. Mong, and G. Refael, Quantum dynamics of thermalizing systems, *Physical Review B* **97**, 035127 (2018).
- [130] T. Rakovszky, C. von Keyserlingk, and F. Pollmann, Dissipation-assisted operator evolution method for capturing hydrodynamic transport, *arXiv preprint arXiv:2004.05177* (2020).
- [131] T. K. Kivorning, L. Herviou, and J. H. Bardarson, Time-evolution of local information: thermalization dynamics of local observables, *arXiv preprint arXiv:2105.11206* (2021).
- [132] C. von Keyserlingk, F. Pollmann, and T. Rakovszky, Operator backflow and the classical simulation of quantum transport, *arXiv preprint arXiv:2111.09904* (2021).
- [133] J. Preksill, *Quantum computation: Chapter 10. Quantum Shannon Theory*.
- [134] E. Witten, A mini-introduction to information theory, *La Rivista del Nuovo Cimento* **43**, 187 (2020).

Appendix A: Useful definitions, operator identities and entropy inequalities

1. Matrix norm

We summarize various matrix norms used in this tutorial. Given an operator O acts on a Hilbert space with dimension d , we denote λ_i as the singular values of O . By definition, λ_i are either positive or zero. We order the singular values so that $\lambda_1 \leq \lambda_2 \leq \dots \leq \lambda_d$. Equivalently, the λ_i are the positive square roots of the eigenvalues of the Hermitian operator $O^\dagger O$. Throughout this tutorial, we use the following conventions for matrix norms,

$$\begin{aligned} \|O\|_1 &= \sum_i \lambda_i = \text{tr} \left(\sqrt{O^\dagger O} \right), \\ \|O\|_2 &= \sqrt{\sum_i \lambda_i^2} = \sqrt{\text{tr}(O^\dagger O)}, \\ \|O\|_\infty &= \lambda_d, \end{aligned} \quad (\text{A1})$$

where $\|O\|_1$ is the trace norm, $\|O\|_2$ is Frobenius norm and $\|O\|_\infty$ is the operator norm, which is the largest singular value of O . We have the inequalities

$$\frac{1}{d} \|O\|_2^2 \leq \|O\|_\infty^2. \quad (\text{A2})$$

2. Entropy inequalities

- Cauchy-Schwarz inequality

$$\langle \psi | \phi \rangle \leq \sqrt{\langle \psi | \psi \rangle \langle \phi | \phi \rangle} \quad (\text{A3})$$

- subadditivity

$$S(A) + S(B) \geq S(AB) \quad (\text{A4})$$

- triangle inequality

$$|S(A) - S(B)| \leq S(AB) \quad (\text{A5})$$

- strong subadditivity

$$S(AB) + S(BC) \geq S(ABC) + S(B) \quad (\text{A6})$$

- Pinsker's inequality

$$\text{tr} \rho_1 (\log_2 \rho_1 - \log_2 \rho_2) \geq \frac{1}{2 \ln 2} \|\rho_1 - \rho_2\|_1^2 \quad (\text{A7})$$

We recommend the lecture notes by Preskill on quantum computation, chapter 10 [133] and the introductory article by Witten [134] for a brief description of the entropy inequalities.

3. Operator identities

Now we summarize some operator identities that are repeatedly used throughout this article. For a quantum many-body system with dimension d , a complete operator basis \mathcal{S} for a quantum system satisfy the following condition

$$\frac{1}{d} (\mathcal{S}^\dagger \mathcal{S}') = \delta_{\mathcal{S} \mathcal{S}'}, \quad \frac{1}{d} \sum_{\mathcal{S}} \mathcal{S}_{ab}^\dagger \mathcal{S}_{cd} = \delta_{ad} \delta_{bc}, \quad (\text{A8})$$

Ensemble average of $d \times d$ Haar random unitary matrix obeys

$$\begin{aligned} \mathbb{E} (U_{a'a} U_{b'b}^*) &= \frac{1}{d} \delta_{a'b'} \delta_{ab} \\ \mathbb{E} (U_{a'a} U_{b'b}^* U_{c'c} U_{d'd}^*) &= \frac{1}{d^2 - 1} (\delta_{a'b'} \delta_{c'd'} \delta_{ab} \delta_{cd} + \delta_{a'd'} \delta_{b'c'} \delta_{ad} \delta_{bc}) \\ &\quad - \frac{1}{d(d^2 - 1)} (\delta_{ab} \delta_{cd} \delta_{a'd'} \delta_{b'c'} + \delta_{a'b'} \delta_{c'd'} \delta_{ad} \delta_{bc}). \end{aligned} \quad (\text{A9})$$

Appendix B: Operator strings and OTOC in qudit systems and majorana systems

1. OTOC in qudit system

As a generalization of the Pauli matrix, a complete basis of operators in q dimension Hilbert space can be

defined as

$$\sigma^{mn} = \sum_{k=0}^{q-1} |k\rangle \langle k+m| \exp \left(i \frac{2\pi}{q} kn \right) \quad (\text{B1})$$

This is a unitary but not Hermitian basis. These operators obey

$$\frac{1}{q} \text{tr} (\sigma^{kn\dagger} \sigma^{k'n'}) = \delta_{kk'} \delta_{nn'} \quad (\text{B2})$$

They also satisfy the completeness relation

$$\frac{1}{q} \sigma_{ab}^{\dagger, mn} \sigma_{cd}^{mn} = \delta_{ad} \delta_{bc}. \quad (\text{B3})$$

Similar to the qubits system, a Heisenberg operator in the system containing multiple qudits can be expanded in the operator string basis

$$W(t) = \sum_{\mathcal{S}} \alpha(\mathcal{S}) \quad (\text{B4})$$

where \mathcal{S} is a product of operators σ_r^{mn} acting on each qudits. Using the completeness relation, one can show that the averaged OTOC is

$$\frac{1}{q^2} \frac{1}{q^N} \sum_{mn} \text{tr} (W^\dagger(t) \sigma_r^{mn\dagger} W(t) \sigma_r^{mn}) = \sum_{\mathcal{S}, \mathcal{S}'=I} |\alpha(\mathcal{S})|^2. \quad (\text{B5})$$

It measure the probability that the operator on the r th qubit in the $W(t)$ is the identity. From this relation, one can also show that the averaged squared commutator

$$\frac{1}{q^2 - 1} \sum_{mn} \frac{1}{q^N} \| [W(t), \sigma_r^{mn}] \|^2 = \frac{2q^2}{q^2 - 1} \sum_{\mathcal{S}(r) \neq I} |\alpha(\mathcal{S})|^2 \quad (\text{B6})$$

In the scrambling limit, the operator string reaches local equilibrium where each onsite operator is equally probable, and the averaged squared commutator reaches 2.

2. OTOC in majorana systems

Consider a system of N majorana fermions, labeled as χ_α , which obeys the commutation relation $\{\chi_\alpha, \chi_\beta\} = \delta_{\alpha\beta}$. A conventional basis for operators in this system is the majorana string

$$\mathcal{S} = i^{m(m-1)/2} 2^{m/2} s_1 s_2 \cdots s_N \quad (\text{B7})$$

where s_r can be either χ_r or I_r and m counts the number of majorana in the string. The factor $i^{m(m-1)/2}$ is to ensure the Hermiticity of \mathcal{S} and $2^{m/2}$ is to ensure the normalization $\text{tr} \mathcal{S}^2 = \text{tr} I$. The Heisenberg operator $\chi(t)$ can be expanded in this basis as

$$\chi(t) = \frac{1}{\sqrt{2}} \sum \alpha(\mathcal{S}, t) \mathcal{S}. \quad (\text{B8})$$

The expansion only contains odd number of majoranas because the fermion parity is conserved. The unitary quantum dynamics ensures that $\sum_{\mathcal{S}} |\alpha(\mathcal{S})|^2 = 1$ for all time. Therefore $|\alpha(\mathcal{S})|^2$ can be interpreted as a probability distribution. Then the OTOC can be written as

$$F(r, t) = \frac{1}{\text{tr} I} \text{tr}(\chi(t) \chi_r \chi(t) \chi_r) = -\frac{1}{4} + \frac{1}{2} \sum_{s_r = \chi_r} |\alpha(\mathcal{S})|^2. \quad (\text{B9})$$

It is directly related to the probability that the majorana operator χ_r appears in the operator string. In the scrambling limit, the majorana operator and the identity operator has the same probability to appear and $F(r, t)$ approaches 0. In the majorana system, the counterpart of the squared commutator is the squared anti-commutator

$$C(r, t) = \frac{4}{\text{tr} I} \text{tr}(\{\chi(t), \chi_r\} \{\chi(t), \chi_r\}) = 4 \sum_{s_r = \chi_r} |\alpha(\mathcal{S})|^2. \quad (\text{B10})$$

In the scrambling limit, $C(r, t)$ approaches 2, the same values as that in the qudit system.

Appendix C: Lieb-Robinson bound

This appendix reviews an elementary proof of a Lieb-Robinson bound for a simple one-dimensional spin to give a sense of how it works. The analysis follows a discussion of Osborne. Let's assume the Hamiltonian can be written as a sum of terms h_r that act on sites r and $r+1$. This can always be done coarse-graining any finite range interaction. Let the operator norm of h_r be J , which measures the local energy scale of the Hamiltonian.

Consider an operator W located at site r_0 . The goal of Lieb-Robinson is to upper bound how far from r_0 this operator can spread after time t . The rough idea is to consider a series of approximations to $W(t)$ which involve truncating more and more distant terms in the Hamiltonian. These truncations then converge, roughly speaking, to $W(t)$ while also giving bound on the spreading.

Denote the restriction of H to the interval $[r-\ell, r+\ell]$ by H_ℓ , which means keeping only terms from H that are fully supported on the interval. The restricted Hamiltonian reads

$$H_\ell = \sum_{r=r_0-\ell+1}^{r_0+\ell-1} h_r \quad (\text{C1})$$

with the dependence on r_0 suppressed. Using the H_ℓ , define the sequence of Heisenberg operators W_ℓ via

$$W_\ell = e^{iH_\ell t} W e^{-iH_\ell t}. \quad (\text{C2})$$

To quantitatively estimate how these terms differ from each other, define the norms α_ℓ by

$$\alpha_\ell = \|W_\ell - W_{\ell-1}\| \quad (\text{C3})$$

with $\alpha_0 = \|W\|$. In terms of these, it is possible to upper bound objects of the form $\|W_\ell - W_{\ell'}\|$ as

$$\|W_\ell - W_{\ell'}\| \leq \sum_{j=\ell'+1}^{\ell} \alpha_j \quad (\text{C4})$$

by repeatedly adding and subtracting $W_{\ell''}$ s and using the triangle inequality.

The α_ℓ s are determined using a differential equation,

$$\frac{d}{dt} \alpha_\ell \leq \left\| \frac{d(W_\ell - W_{\ell-1})}{dt} \right\|. \quad (\text{C5})$$

Using the invariance of the norm under unitary transformations, the right hand side can be equivalently written as

$$\left\| \frac{d}{dt} (U_{\ell+1} W_\ell U_{\ell+1}^\dagger - W) \right\| \quad (\text{C6})$$

which is

$$\|[-iH_{\ell+1}, W_\ell] + [iH_\ell, W_\ell]\| = \|[H_{\ell+1} - H_\ell, W_\ell]\|. \quad (\text{C7})$$

The next step identifies $H_{\ell+1} - H_\ell$ with $h_{r_0+\ell} + h_{r_0-\ell}$, since these are the only new terms in $H_{\ell+1}$ fully supported on $[r_0 - \ell - 1, r_0 + \ell + 1]$ but not fully on $[r_0 - \ell, r_0 + \ell]$. We also use the fact that $W_{\ell-1}$ has no non-trivial support on $r_0 \pm \ell$ or $r_0 \pm (\ell + 1)$ and hence commutes with $H_{\ell+1} - H_\ell$. Thus the right hand side of the α_ℓ differential equation can be taken to be

$$\|[H_{\ell+1} - H_\ell, W_\ell - W_{\ell-1}]\| \leq 4J \|W_\ell - W_{\ell-1}\| = 4J \alpha_{\ell-1}. \quad (\text{C8})$$

Using $\|AB\| \leq \|A\| \|B\|$ and the triangle inequality, one has

$$\frac{d\alpha_\ell}{dt} \leq 4J \alpha_{\ell-1}. \quad (\text{C9})$$

The factor of four is a crude upper bound that takes into account both $h_{r_0+\ell}$ and $h_{r_0-\ell}$ which both appear twice due to the commutator.

Now we solve the upper limit of this system of differential equations with the initial condition that $\alpha_0 = \|W\|$ and $\alpha_{\ell>0}(t=0) = 0$. The result is

$$\alpha_\ell(t) \leq \|W\| \frac{(4Jt)^\ell}{\ell!}. \quad (\text{C10})$$

This result is almost the end of the calculation. The remaining thing to do is to estimate the difference between W_ℓ and the true $W(t)$. This is

$$\|W(t) - W_\ell\| \leq \sum_{j=\ell+1}^{\infty} \alpha_j \leq \sum_{j=\ell+1}^{\infty} \|W\| \frac{(4Jt)^j}{j!}. \quad (\text{C11})$$

There are various ways to treat this infinite sum. For $\ell \gg 4Jt$, the simplest estimate is to say that it cannot be much larger than its first term, which is quite

small. More precisely, the ratio of term j to term $j+1$ is $\frac{4Jt}{j+1} \leq \frac{4Jt}{\ell+2}$, so making even a crude approximation using a geometric series in $\frac{4Jt}{\ell+2}$ converges to something order one times the first term. After using Stirling's approximate for large ℓ , the first term is

$$\|W\| \frac{(4Jt)^{\ell+1}}{(\ell+1)!} \approx \|W\| \left(\frac{4eJt}{\ell+1} \right)^{\ell+1}. \quad (\text{C12})$$

This result corresponds to roughly the ℓ th order in perturbation theory when expanding $W(t)$ in a Taylor series. Physically, it will describe the commutator dynamics for sufficiently small t and large ℓ .

Neglecting the difference between ℓ and $\ell+1$, the first term is order one when $\ell = 4eJt$. Setting $\ell_0 = 4eJt$, the first term can be written as

$$e^{\ell \log \frac{\ell_0}{\ell}}. \quad (\text{C13})$$

Using $-1 \geq -1 + \log \frac{\ell_0}{\ell}$ (valid for $\ell \geq \ell_0$) and integrating both sides from ℓ_0 to ℓ , it follows that

$$-(\ell - \ell_0) \geq \ell \log \frac{\ell_0}{\ell}. \quad (\text{C14})$$

The left hand side is the first order expansion of the right hand side in $\ell - \ell_0$, so the inequality states that going beyond first order only decreases the value. Hence

$$e^{\ell \log \frac{\ell_0}{\ell}} \leq e^{-(\ell - \ell_0)}, \quad (\text{C15})$$

or, using $\ell_0 = 4eJt$,

$$\|W(t) - W_\ell\| \leq \|W\| f(t) e^{4eJt - \ell}. \quad (\text{C16})$$

Here $f(t)$ is a polynomial prefactor that I wasn't careful about because it doesn't affect the basic exponential scaling. Note that the bound is definitely not tight at very large ℓ , since $1/\ell!$ decreases faster than $e^{-\ell}$. The bound is also trivial once $\ell < \ell_0$ because the right hand side is growing exponentially while the left hand side is bounded by $2\|W\|$.

Having established that W_ℓ is close to $W(t)$ for $\ell \gg Jt$, remains to upper bound the commutator. The idea is straightforward: If an operator V is a distance r from W , then an upper bound on the commutator $\|[W(t), V]\|$ is obtained by approximating W with $W_{\ell=r-1}$ since W_{r-1} exactly commutes with V . First add and subtract W_{r-1} inside the norm to give

$$\|[W(t), V]\| = \|[W(t) - W_{r-1} + W_{r-1}, V]\|, \quad (\text{C17})$$

and then use $[W_{r-1}, V] = 0$ and the bound on $\|W(t) - W_{r-1}\|$ to obtain

$$\|[W(t), V]\| \leq 2\|V\| \|W(t) - W_{r-1}\|. \quad (\text{C18})$$

Using the upper bound above, this is

$$\|[W(t), V]\| \leq 2\|V\| \|W\| f(t) e^{4eJt - r}, \quad (\text{C19})$$

which is Eq. (13) in the main text.